Opposing actions of septins and Sticky on Anillin promote the transition from contractile to midbody ring

Nour El Amine,[1,2] Amel Kechad,[1,2] Silvana Jananji,[1] and Gilles R.X. Hickson[1,2]

[1]Centre de Cancérologie Charles Bruneau, Centre Hospitalier Universitaire Sainte-Justine Centre de Recherche, Montréal, Québec H3T 1C5, Canada
[2]Département de Pathologie et Biologie Cellulaire, Université de Montréal, Montréal, Québec H3C 3J7, Canada

During cytokinesis, closure of the actomyosin contractile ring (CR) is coupled to the formation of a midbody ring (MR), through poorly understood mechanisms. Using time-lapse microscopy of *Drosophila melanogaster* S2 cells, we show that the transition from the CR to the MR proceeds via a previously uncharacterized maturation process that requires opposing mechanisms of removal and retention of the scaffold protein Anillin. The septin cytoskeleton acts on the C terminus of Anillin to locally trim away excess membrane from the late CR/nascent MR via internalization, extrusion, and shedding, whereas the citron kinase Sticky acts on the N terminus of Anillin to retain it at the mature MR. Simultaneous depletion of septins and Sticky not only disrupted MR formation but also caused earlier CR oscillations, uncovering redundant mechanisms of CR stability that can partly explain the essential role of Anillin in this process. Our findings highlight the relatedness of the CR and MR and suggest that membrane removal is coordinated with CR disassembly.

Introduction

During cytokinesis of animal cells, an actomyosin-based contractile ring (CR) forms and drives the ingression of a cleavage furrow that bisects the cell at the midpoint of the microtubule-based spindle (Glotzer, 2005; Eggert et al., 2006; Barr and Gruneberg, 2007; Pollard, 2010; Green et al., 2012). The CR is a dynamic, membrane-bound structure that requires continuous Rho-dependent signaling (Bement et al., 2005) and contains many cytoskeletal proteins, including actin, myosin II, Anillin, septins, and their regulators. CR closure occurs via disassembly and proceeds until reaching a diameter of 1–2 µm (Schroeder, 1972; Carvalho et al., 2009). The CR then transforms itself into the midbody ring (MR), a long-lived, dense structure that forms around the center of the midbody as it matures from the antiparallel midzone microtubules that become compacted during CR closure (Mullins and Biesele, 1977; Hu et al., 2012). The MR is essential for cementing the efforts of the CR and for specifying where, and presumably when, abscission ultimately occurs (Steigemann and Gerlich, 2009; Green et al., 2012).

Correspondence to Gilles R.X. Hickson: gilles.hickson@umontreal.ca

Abbreviations used in this paper: ActBD, actin-binding and -bundling domain; AHD, Anillin homology domain; CD, central domain; Cit-K, Citron kinase; CR, contractile ring; dsRNA, double-stranded RNA; FP, fluorescent protein; KD, kinase dead; mCh, mCherry; MR, midbody ring; MRLC, myosin regulatory light chain; MyoBD, myosin-binding domain; PH, Pleckstrin homology; PHD, PH domain; Pnut, Peanut; Tum, Tumbleweed.

Our previous work showed that the transition from the CR to the MR requires the scaffold protein Anillin (Kechad et al., 2012). Anillin-depleted CRs are unstable and oscillate back and forth across the equator (Straight et al., 2005; Zhao and Fang, 2005; Hickson and O'Farrell, 2008b; Piekny and Glotzer, 2008; Goldbach et al., 2010), but even CRs that do not oscillate fail to close completely and fail to form a stable MR (Kechad et al., 2012). Anillin can bind many other cytokinesis proteins, including F-actin (Field and Alberts, 1995), myosin (Straight et al., 2005), septins (Oegema et al., 2000; Field et al., 2005; Liu et al., 2012), and RacGAP50c (D'Avino et al., 2008; Gregory et al., 2008), among others (Hickson and O'Farrell, 2008a; D'Avino, 2009; Piekny and Maddox, 2010). It remains unclear how Anillin acts to dampen the inherent instabilities of cleavage furrows (Dorn and Maddox, 2011; Sedzinski et al., 2011), and how it subsequently guides MR formation after CR closure.

Here, we show that the CR gives rise to the MR via a previously uncharacterized maturation process involving opposing mechanisms acting on Anillin: the septin Peanut (Pnut) acts with the C terminus of Anillin to locally remove membrane,

The Rockefeller University Press $30.00
J. Cell Biol. Vol. 203 No. 3 487–504
www.jcb.org/cgi/doi/10.1083/jcb.201305053

whereas the Citron kinase (Cit-K) Sticky acts to retain the N terminus of Anillin at ring structures. Furthermore, Pnut and Sticky redundantly stabilize the earlier CR. The data lead to the proposal that septin-dependent removal of membrane-associated Anillin during disassembly of the actomyosin ring contributes to CR stability and closure, whereas Sticky-dependent retention of Anillin also contributes to CR stability and limits the removal of Anillin from the mature MR.

Results

Maturation of the MR is accompanied by removal and retention of Anillin

To better define the process of MR formation and maturation, we have monitored the localization of Anillin-GFP (Hickson and O'Farrell, 2008b) using time-lapse spinning-disc confocal microscopy. Anillin-GFP localized to the CR and MR throughout cytokinesis and to the MR remnant that remained associated with one of the sister cells after abscission (Fig. 1 A). Induced expression of Anillin-GFP under the control of the metallothionein promoter resulted in a fourfold overexpression of Anillin (Fig. S1, A–C). This fully rescued for loss of endogenous Anillin (Hickson and O'Farrell, 2008b) and had no consequence on the duration of furrowing or the timing of abscission when compared with other markers, such as GFP-tubulin or the myosin regulatory light chain (MRLC) Spaghetti squash–GFP (myosin-GFP; unpublished data). However, during formation of the MR, we observed a gradual thinning of the MR structure that was unexpectedly accompanied by extrusion and internalization of Anillin-GFP (Fig. 1, A–C). Extrusion originated from blebs or tubules that formed either at late stages of furrowing (Fig. 1 B and Video 1) or at the nascent MR soon after furrowing (Fig. 1 C). The extruded material persisted for several minutes and in some cases was clearly shed completely from the cell (Fig. 1, B and C, arrowheads). During internalization, Anillin-containing structures budded from the cytokinetic apparatus and were internalized into the cytoplasm as punctate vesicular structures (Fig. 1 E and Video 2). At the nascent MR, Anillin-FP sometimes labeled plasma membrane folds that had been gathered up during CR closure (Fig. S1 E). Such plasma membrane folds were also evident by EM (Fig. S1 F). Mature MRs, however, were more uniform in shape, had more closely opposed plasma membranes, and exhibited a double ring ultrastructure with a more electron-dense outer layer and a less dense inner layer (Fig. S1 F), similar to that described for intercellular canals in *Drosophila melanogaster* embryos (Haglund et al., 2011). The extruded structures labeled with a plasma membrane marker, myristoylated palmitoylated–GFP (myrpalm-GFP; Fig. S1), although this revealed many additional plasma membrane protrusions associated with the nascent MR that did not contain Anillin–fluorescent protein (FP; Fig. S1 G). These membrane protrusions accumulated during furrowing but then gradually dissipated during MR maturation, indicating that excess plasma membrane is gathered by the CR and then removed from the nascent MR (Fig. S1 H).

Extrusion/shedding and internalization of Anillin occurred during the ∼1-h period that followed CR closure and coincided with a progressive decline in total Anillin-FP intensity measured at the nascent MR (n = 20; Fig. 1 E). Beyond this time, the appearance and intensity of MRs remained constant until after abscission. We examined the dynamic nature of Anillin-GFP at different stages of MR biogenesis using FRAP. When the entire MR region was bleached within 15 min of CR closure (Fig. 1 F, top), 30 ± 13% of Anillin-GFP fluorescence recovered within 4 min (n = 16; Fig. 1 G). However, when bleached >45 min after CR closure (Fig. 1 F, bottom), only 10 ± 6% recovery was observed within 4 min (n = 9; Fig. 1 G), indicating that the potential to restore Anillin to the MR declined as it matured. Photoconversion of an Anillin-Dendra2-FP revealed that the recovery occurred preferentially at the flanking regions, whereas less exchange occurred at the central region of the MR (Fig. S1 H). We conclude that nascent MRs mature over the course of ∼1 h into stable MRs, during which they progressively extrude, shed, and internalize Anillin.

Nascent MRs shed numerous cytokinesis proteins but not F-actin

We wished to determine whether other cytokinesis proteins were also shed with Anillin during MR maturation. Immunofluorescence analysis revealed that the septin, Pnut (Fig. 2 A), and Rho1 (Fig. 2 B) were also enriched on the extruded membranes. Similarly, the Cit-K, Sticky-FP, was extruded with Anillin-FP (Fig. 2 C), as were the components of the centralspindlin complex, RacGAP50C/Tumbleweed (Tum)-FP (Fig. 2 D) and the kinesin-6 motor Pavarotti-FP (Fig. 2 E). Aurora B–GFP, which also localizes primarily to the central spindle and midbody microtubules (Fig. 2 F), was also extruded from the center of the midbody soon after CR closure.

Cells expressing myosin-GFP showed no evidence of extrusion, shedding, or internalization (Fig. 2 G), unless Anillin-mCherry (mCh) was also coexpressed, in which case some myosin-GFP colocalized with shed Anillin-mCh (Fig. 2 H). However, the F-actin probe LifeAct-GFP (Riedl et al., 2008), although enriched at the late CR, did not colocalize with extruded Anillin-FP (Fig. 2 I). Phalloidin staining of fixed cells also revealed that the extruded Anillin-positive membranes were labeled poorly for F-actin (Fig. 2 J). Thus, although numerous key components of the cytokinesis machinery were removed via extrusion and shedding, actin was specifically not. We next designed experiments to further understand the mechanisms of Anillin removal from the late CR/nascent MR.

Shedding from the nascent MR requires Anillin but not ESCRT-III or the proteasome

Aurora B–GFP and Tum-GFP showed evidence of shedding even when Anillin was not overexpressed (Fig. 3, A and C). We therefore used these markers to test whether Anillin was itself required for shedding. In Anillin-depleted cells, Aurora B–GFP was no longer extruded compared with controls but still disappeared from the cleavage site over a similar time course to controls (n > 20; Fig. 3, A and B). Similarly, no evidence of Tum-GFP extrusion was observed from Anillin-depleted late CRs/nascent MRs (n > 20; Fig. 3, C and D). Thus, Anillin is

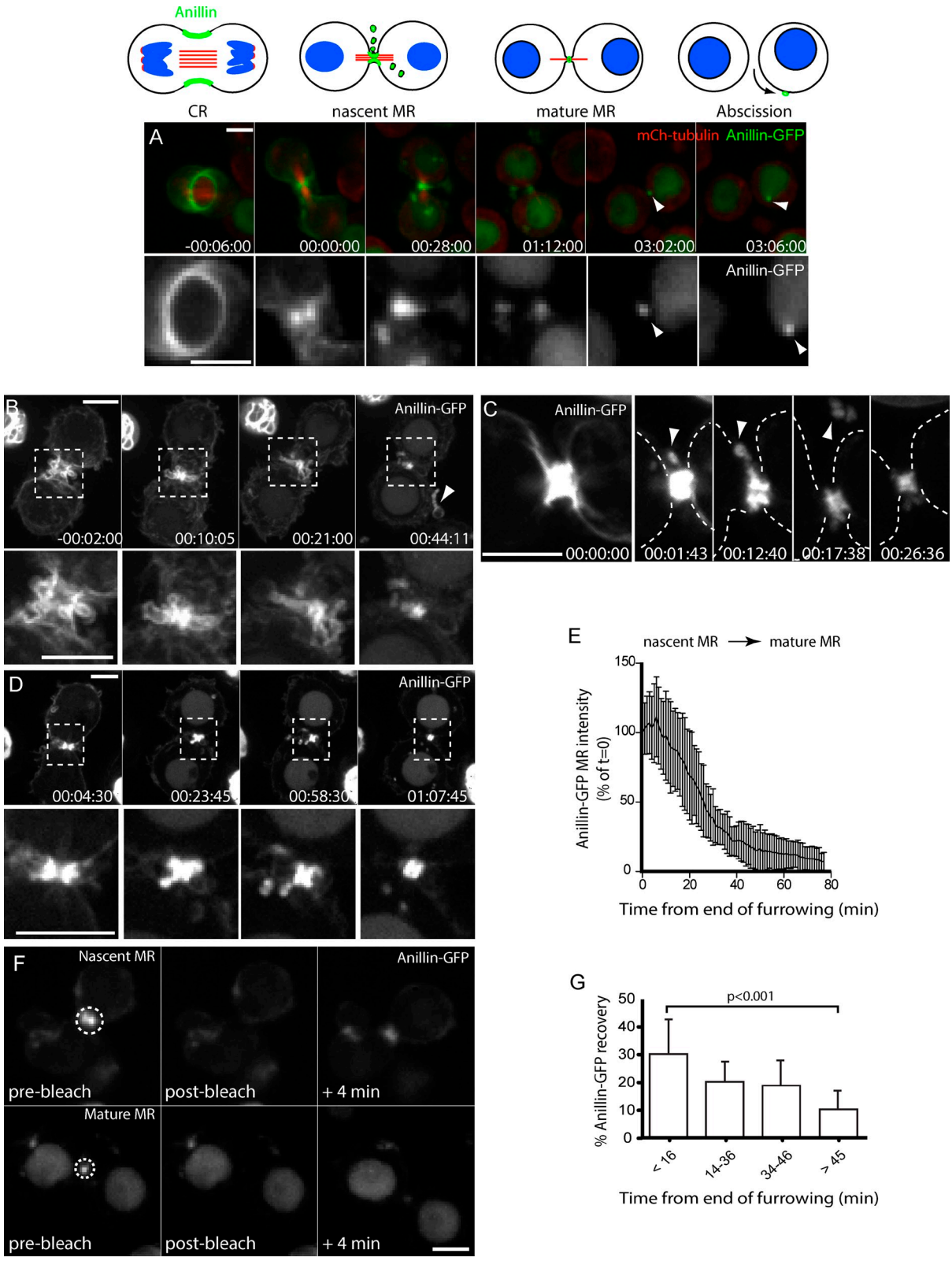

Figure 1. **Maturation of the MR is accompanied by both removal and retention of Anillin.** (A) Time-lapse sequence of a cell expressing Anillin-GFP and mCh-tubulin (40× objective). Arrowheads mark the mature MR before and after abscission MR release. (B–D) Time-lapse sequence of cells expressing Anillin-GFP and mCh-tubulin (not depicted) acquired with 40× objective, showing extrusion and shedding (B and C) and internalization (D). Boxed regions in B and D are shown magnified at the bottom; dashed lines in C mark the cell boundary; arrowheads mark shed material. (E) Relative Anillin-GFP fluorescence (sum intensity) at nascent MRs measured from the end of furrowing (means ± SD; $n = 20$). (F) FRAP experiments of nascent and mature MRs, showing images acquired immediately before (prebleach), after (bleach), and 4 min after high-intensity illumination of the outlined region of interest (63× objective and 2 × 2 camera binning). (G) The percent recovery of GFP fluorescence within 4 min of bleaching is shown for MRs of different ages ($n = 9$–17 each, means ± SD). P-value is for an unpaired t test. Times are hours, minutes, and seconds from the end of furrowing. Bars, 5 µm. See also Videos 1 and 2.

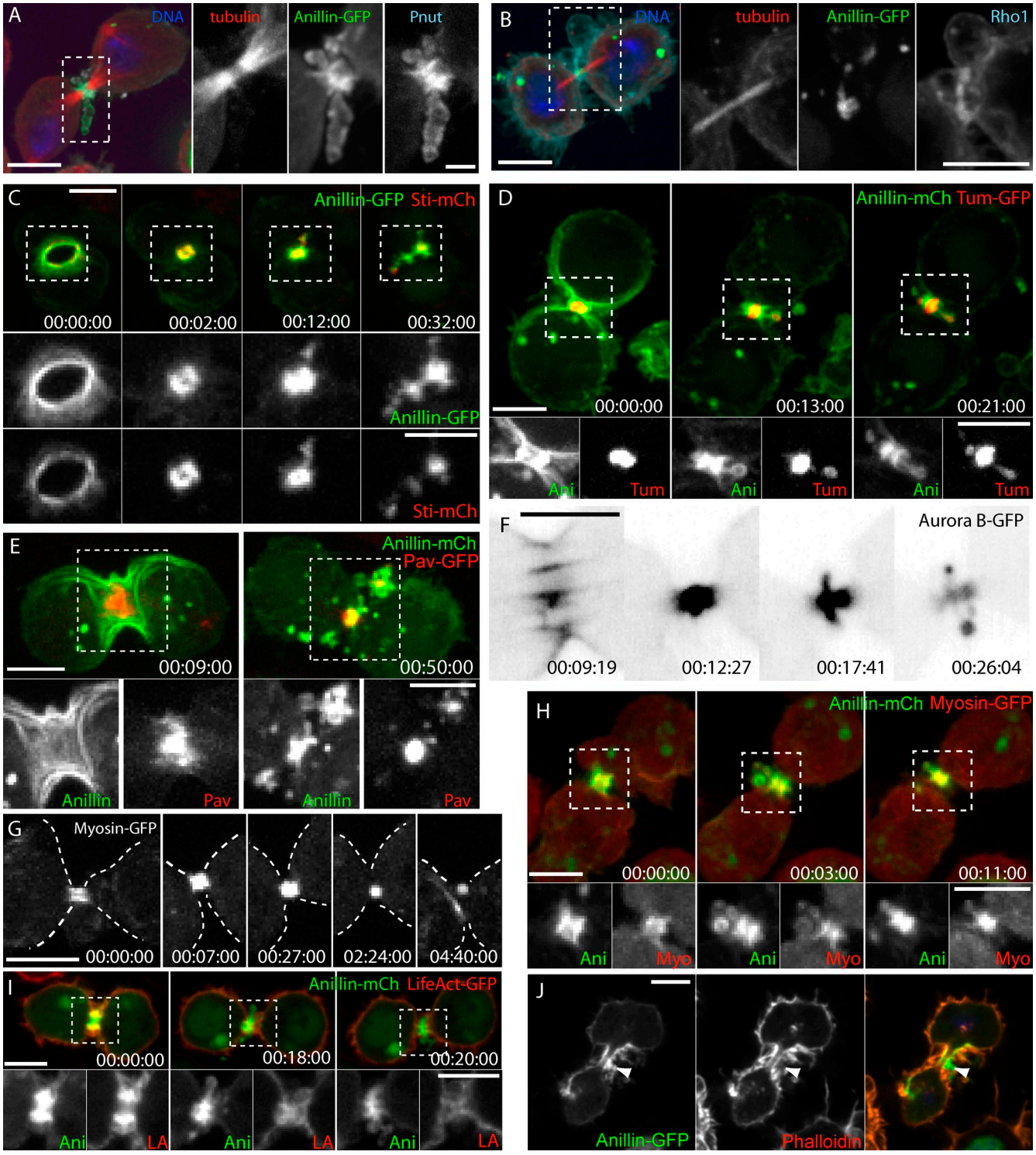

Figure 2. **Nascent MRs shed numerous CR components, except F-actin.** (A and B) Fixed cells expressing Anillin-GFP and tubulin-mCh stained for anti-Pnut (A) and anti-Rho1 (B) by immunofluorescence. Separated channels of boxed regions are shown magnified on the right. (C) Cell expressing Anillin-GFP and Sticky (Sti)-mCh. (D) Cell expressing Anillin-mCh and Tum-GFP. (E) Cell expressing Anillin-mCh and Pavarotti (Pav)-GFP. (F) Inverted look-up table of the nascent MR of an Aurora B–GFP-expressing cell. (G) The nascent MR of a myosin-GFP–expressing cell. Dashed lines mark the cell boundary. (H) The nascent MR of a cell expressing myosin-GFP (Myo) and Anillin-mCh (Ani). (I) The nascent MR of a cell expressing LifeAct-GFP (LA) and Anillin-mCh. (C, D, E, H, and I) Separated channels of boxed regions are shown magnified at the bottom. (J) The nascent MR of a cell expressing Anillin-GFP fixed and stained with rhodamine-phalloidin. Arrowhead points to an extrusion enriched in Anillin-GFP but lacking actin. Times are hours, minutes, and seconds. Bars: (A [main image] and B–J) 5 µm; (A, magnified images) 1 µm. See also Video 3.

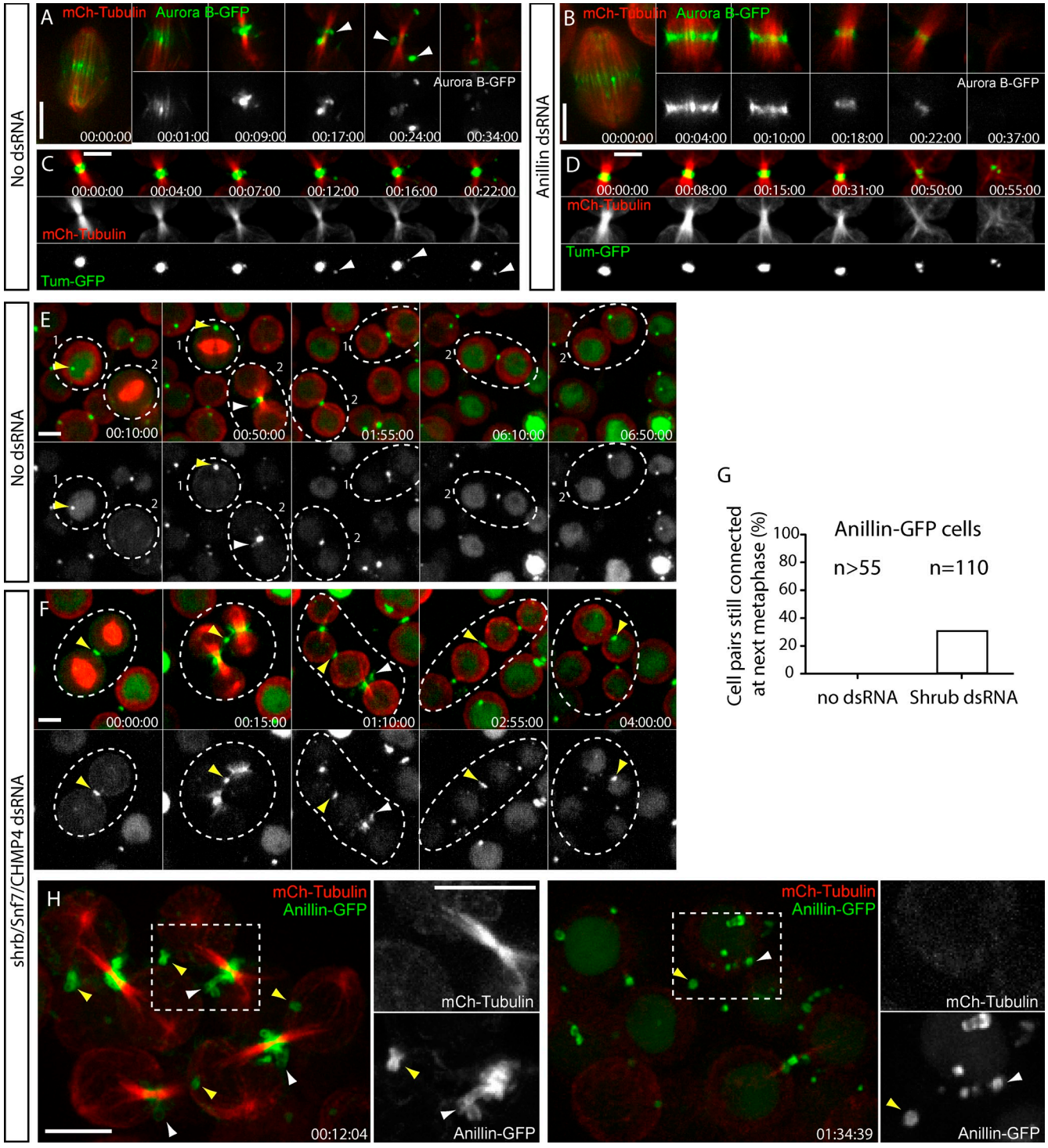

Figure 3. **Shedding from the nascent MR requires Anillin but not ESCRT-III.** (A and B) Time-lapse sequence of cells expressing Aurora B–GFP and mCh-tubulin after a 3-d incubation without (A) or with (B) Anillin dsRNAs, acquired with a 100×, 1.4 NA objective. Arrowheads in A mark shedding events. (C and D) Time-lapse sequence of cells expressing Tum-GFP and mCh-tubulin after a 3-d incubation without (C) or with (D) Anillin dsRNAs. Arrowheads in C mark shedding events. (E and F) Selected frames from a time-lapse sequence of Anillin-GFP cells after a 4-d incubation without (E) or with (F) *shrub* dsRNAs, acquired with a 40× objective. Dotted circles highlight sister cells; yellow arrowheads mark mature MRs/MR remnants from previous divisions; and white arrowheads mark MRs from the current division. (G) Quantification of Anillin-GFP–expressing cells that have failed to undergo abscission and thus remain paired at metaphase in control and Shrub-depleted cells. Data are from two independent experiments. (H) Selected frames from a time-lapse sequence of Anillin-GFP cells, acquired with a 100× objective, after a 4-d incubation with *shrub* dsRNAs. Boxed regions are shown magnified and with separated channels on the right; yellow arrowheads mark mature MRs from previous divisions; and white arrowheads mark nascent MRs from the current division that are shedding Anillin-GFP. Times are given in hours, minutes, and seconds. Bars, 5 µm. See also Video 4.

required for extrusion, although we note that this may reflect a direct requirement for Anillin in the extrusion process, an indirect consequence of the requirement for Anillin in complete CR closure (Kechad et al., 2012), or both.

The membrane topology during extrusion/shedding is the same as the abscission event that occurs later. We therefore tested whether shedding, like abscission, requires ESCRT-III complexes. A 3–4-d depletion of Shrub, the *Drosophila* orthologue of CHMP4B, a key ESCRT-III component (Elia et al., 2011; Carlton et al., 2012), delayed abscission well beyond the 3 h and 48 s ± 1 h and 57 s (mean ± SD; n = 12) observed for untreated controls, although cells never became binucleated. Shrub-depleted cells remained paired for so long that they could not be reliably followed from furrowing to abscission, as the cells, being poorly adherent, would often move out of the imaging field over time. However, we noted that 30% of Shrub-depleted cells initiated cytokinesis while still connected to their sister cells from the previous attempt (n = 110 pairs; Fig. 3, E–G), whereas control cells had always undergone abscission before reaching the next metaphase (n > 55 pairs). Daisy chains of Shrub-depleted cells were sometimes observed, consistent with abscission failure in multiple rounds of division. Even in the most extreme cases, normal MR maturation was observed, including extrusion, shedding, and internalization of Anillin-GFP (Fig. 3 H, Fig. S2 A, and Video 4). Similar results were obtained upon depletion of dIST1 (unpublished data), another ESCRT-III component required for cytokinesis (Agromayor et al., 2009). Thus, ESCRT-III is required for abscission, as expected, but not for MR maturation.

Human Anillin is subject to anaphase-promoting complex/cyclosome–mediated degradation (Zhao and Fang, 2005). We tested whether degradation of *Drosophila* Anillin might contribute to its decline during MR maturation, by treating cells expressing Anillin-GFP with the proteasome inhibitor MG132. When added early in mitosis, 5 µM MG132 induced widespread metaphase arrest, as expected. Cells that successfully underwent the metaphase/anaphase transition during the 5 min before or after MG132 addition, however, furrowed normally (Fig. S2 B). However, although untreated control cells typically exhibited a net loss of Anillin-GFP soon after the end of furrowing, MG132-treated furrows accumulated Anillin-GFP during the subsequent 15–20 min after closure (n = 14; Fig. S2 C), before exhibiting a profile of net loss that was similar to controls (n = 20; Fig. S2 D) and that ended with a mature MR that was indistinguishable from controls (Fig. S2 E). Extrusion and shedding of Anillin-GFP during MR maturation continued in MG132 (Fig. S2 E). We conclude that proteasomal degradation is not required for extrusion/shedding of Anillin and does not provide a major contribution to the loss of Anillin from the MR during its maturation. However, proteasomal degradation, directly or indirectly, appears to limit the extent or accelerate the rate of Anillin-GFP accumulation at the late CR/nascent MR.

A third population of cells displayed a highly aberrant exit from mitosis that was seen 5–40 min after MG132 addition. Slow and excessive spindle elongation, slow and broad furrows, and a failure of nuclear envelope reformation and/or nuclear import of Anillin-GFP characterized this (Fig. S2 F). We interpret these cells as having degraded only a subset of anaphase-promoting complex/cyclosome substrates, resulting in a partial arrest. Remarkably, most of these cells succeed to a midbody-like stage, although they were not followed until completion.

Collectively, these experiments show that cortical extrusion/shedding during the transition from CR to MR requires Anillin but does not depend on ESCRT-III or the proteasome. We next performed a structure–function analysis of Anillin to further define the requirements for its extrusion and shedding.

Removal of Anillin from the nascent MR is mediated via its C terminus, whereas retention at the mature MR is mediated via its N terminus

Anillin is a large multidomain protein (Fig. 4 A) that can bind to many other cytokinesis proteins (D'Avino, 2009; Piekny and Maddox, 2010). We analyzed truncation mutants lacking domains to determine which mediate its retention and removal at the nascent MR. Anillin-Δactin-binding and -bundling domain (ActBD)-GFP, which lacks the ActBD identified by Field and Alberts (1995), was no longer recruited to the actin-rich cortex in mitosis, similar to the behavior of full-length Anillin-GFP in Latrunculin A–treated cells (Hickson and O'Farrell, 2008b). However, Anillin-ΔActBD-GFP was still recruited to the furrow, nascent MR, and mature MR and exhibited dramatic extrusion and shedding (Fig. S3 A). Anillin-Δmyosin-binding domain (MyoBD)-GFP, which lacks the region adjacent to the ActBD that is homologous to the *Xenopus laevis* myosin II–binding domain (Straight et al., 2005), still localized to the cortex at metaphase, indicating a functional ActBD, and to the CR and nascent MR during cytokinesis (Fig. S3 B). It was also readily extruded and shed and localized to mature MRs, although these appeared smaller than MRs containing full-length Anillin-GFP. Anillin-ΔN, in which the entire N terminus was deleted, leaving only the Anillin homology domain (AHD) and Pleckstrin homology (PH) domain (PHD), was still extruded and shed. Constructs expressing only the AHD or PHD were poorly recruited and showed no evidence of shedding, and deletion of either domain blocked extrusion and shedding. Thus, the C-terminal AHD and PHD are each required and together sufficient for extrusion and shedding.

Conversely, a mutant comprising only the extreme N-terminal domain and the ActBD and MyoBD (Anillin-N) was still recruited to the MR (Fig. S3 C) and behaved similarly to the larger Anillin-ΔC (Kechad et al., 2012). The reciprocal mutants lacking these domains (Anillin-ΔN and Anillin-ΔN with the central domain [CD; Anillin-ΔN+CD]) failed to be retained at the mature MR despite localizing to the nascent MR and readily being extruded and shed (Fig. 4 B). Thus, the Anillin N terminus is both necessary and sufficient for retention at the mature MR.

Coexpressing N- and C-terminal truncations fused to different FPs in the same cells did not alter their respective behaviors and made their differences even more apparent. Fig. 4 B shows Anillin-ΔC-GFP incorporating into the MR without being extruded or internalized, whereas Anillin-ΔN+CD-mCh is completely shed from the nascent MR without incorporating into the mature MR (Fig. 4 B and Video 5). Collectively, our data indicate that distinct mechanisms of removal and retention act

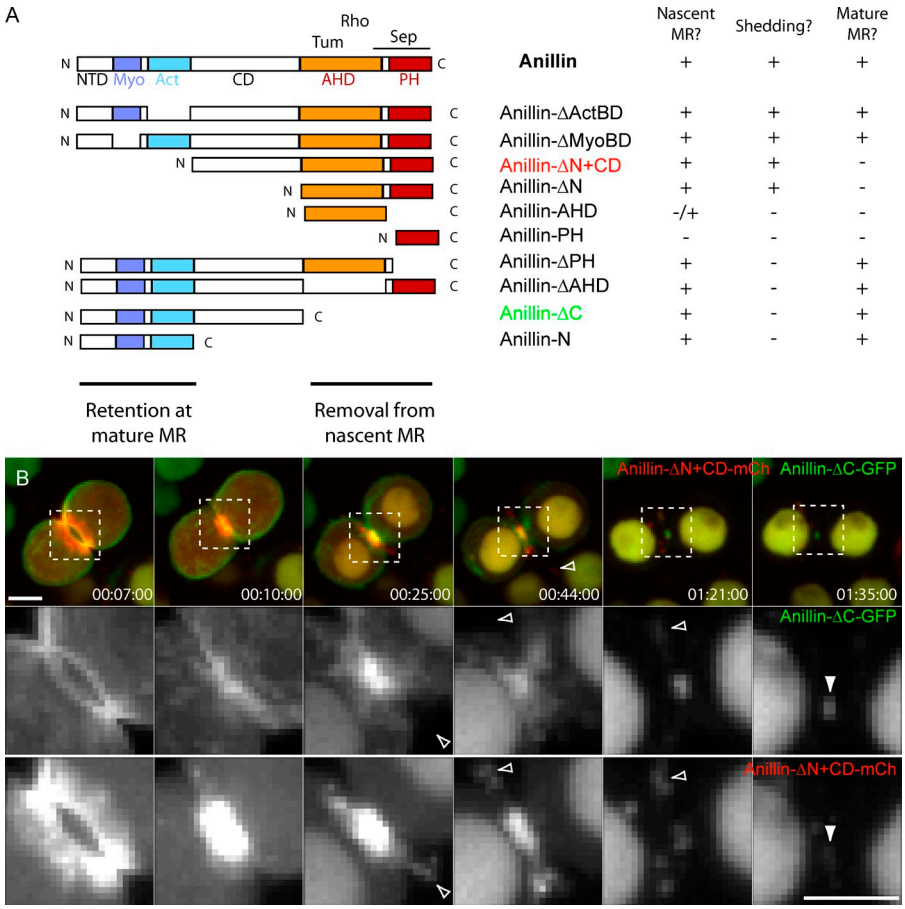

Figure 4. **Removal of Anillin from the nascent MR is mediated via its C-terminal domains, whereas retention requires its N-terminal domains.** (A) Domain organization of Anillin and truncation mutant analyses for their localization to the nascent MR, their ability to be extruded and shed, and their retention at the mature MR. Myo, myosin; Act, actin; NTD, N-terminal domain; Sep, septin; C, C terminus; N, N terminus. (B) Time-lapse sequence of a cell coexpressing Anillin-ΔC-GFP and Anillin-ΔN+CD-mCh. Open arrowheads mark shed material, and closed arrowheads mark the mature MR. Separated channels and magnified images of the boxed regions are shown at the bottom. Times are given in hours, minutes, and seconds. Bars, 5 µm. See also Video 5.

on the C and N termini of Anillin, respectively. We next aimed to better understand the removal mechanisms acting on the C terminus of Anillin.

Maturation of the MR requires septin-dependent removal of Anillin via its C-terminal PHD

The Anillin PHD is known to bind septins (Field and Alberts, 1995; Oegema et al., 2000; Liu et al., 2012) and phosphoinositides (Liu et al., 2012), and septins are required for the recruitment of Anillin-ΔN to the cleavage furrow (Kechad et al., 2012). We further evaluated the requirement for the PHD and septins in Anillin removal during MR maturation. Anillin-ΔPH-FP localized efficiently to the CR and MR but showed little, if any, evidence of extrusion or internalization from the nascent MR, whether or not endogenous Anillin was depleted (Fig. 5, A and C). Anillin-ΔPH-GFP MRs also appeared larger than controls of the same age (Fig. 5 E). Measuring MR volumes over time revealed that Anillin-ΔPH-GFP MRs did not thin to the same extent as Anillin-GFP controls (Fig. 5 F). This effect was dominant, suggesting that the PHD is autonomously required for Anillin removal. A 7–8-d incubation with double-stranded RNAs (dsRNAs) targeting the septin Pnut (Neufeld and Rubin, 1994), which results in >94% depletion in S2 cells (Fig. 5 B), also blocked extrusion/ shedding of Anillin-GFP (Fig. 5 A) and inhibited the thinning of the MR during its maturation (Fig. 5, D–F). Thus, the PHD of Anillin and Pnut are each required for cortical removal during MR maturation.

In the 30% (Anillin-ΔPH-GFP + Anillin dsRNA, $n = 75$) and 34% (Anillin-GFP + Pnut dsRNA) of attempts at cytokinesis that failed, deletion of the PHD or depletion of Pnut produced similar phenotypes: at 1 h and 10 min ± 12 min (mean ± SD; $n = 50$) and 1 h and 23 min ± 33 min (mean ± SD; $n = 50$) after anaphase onset, respectively, the plasma membrane regressed, leaving internal MR-like structures (Fig. 5 G; Kechad et al., 2012). However, in the cells that succeeded, Anillin-ΔPH-FP delayed abscission, which occurred 10 h and 42 min ± 6 h and 7 min (mean ± SD; $n = 50$) after furrowing, whereas Pnut depletion led to premature abscission that occurred 2 h and 19 min ± 0 h and 42 min (mean ± SD; $n = 50$) after furrowing compared with 4 h and 54 min ± 1 h and 36 min (mean ± SD; $n = 75$) for Anillin-FP–expressing controls (Fig. 5 G). Given that the PHD binds both the membrane and septins (Liu et al., 2012), this difference in abscission timing could reflect the difference between loss of septin binding (Pnut depletion) and the additional loss of membrane binding (deletion of the entire PHD). Accordingly, membrane binding by the Anillin PHD may facilitate abscission.

These experiments show that the PHD of Anillin and the septin Pnut are required for the normal thinning of the nascent MR and the extrusion and shedding of membrane-associated Anillin. We next sought to better understand the mechanism of Anillin retention at the MR.

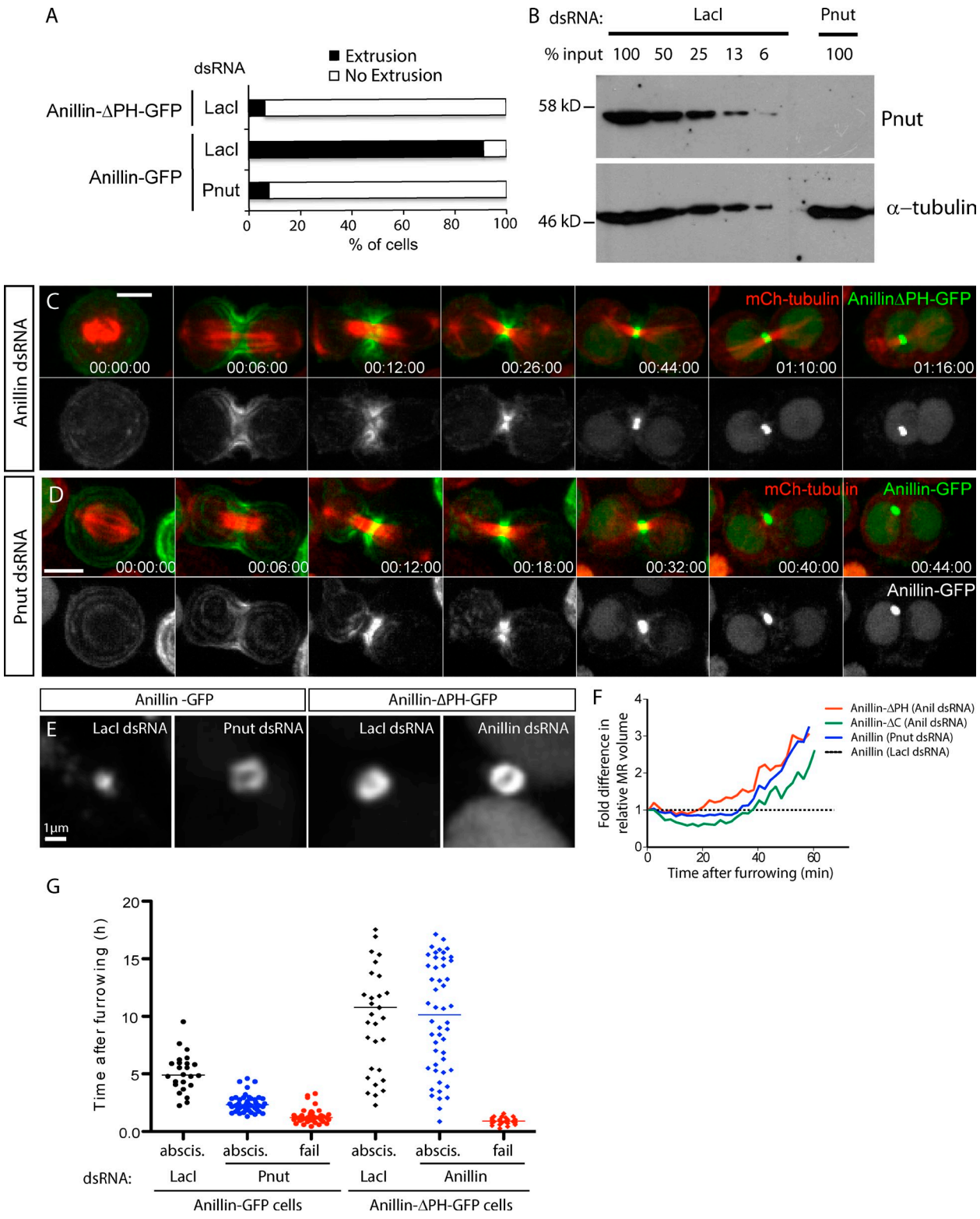

Figure 5. **Proper maturation of the MR requires septin-dependent removal of Anillin via its C-terminal PHD.** (A) Frequency of extrusion from time-lapse sequences of Anillin-ΔPH-GFP and of Anillin-GFP after 8-d Pnut RNAi. (B) Anti-Pnut immunoblot of S2 cell lysates serially diluted after LacI control dsRNA incubation or after Pnut dsRNA incubation; anti-tubulin is the loading control. (C) Time-lapse sequences of cells expressing Anillin-ΔPH-GFP depleted of endogenous Anillin. (D) Time-lapse sequence of an Anillin-GFP–expressing cell after 8-d Pnut RNAi. (E) Representative images of age-matched MR structures from Anillin-GFP or Anillin-ΔPH-GFP cells treated with the indicated dsRNAs. (F) Volume measurements of the nascent MR of cells expressing Anillin-ΔPH-GFP, Anillin-ΔC-GFP, or Anillin-GFP treated with the indicated dsRNAs, from the end of furrowing, normalized at each time point to equivalently aged Anillin-GFP controls (n = 10 per condition from two independent experiments). (G) Timing of abscission (abscis.) or furrow regression (fail) of Anillin-GFP cells treated for 7–9 d with LacI (control, n = 30) or Pnut dsRNAs (n = 75) and of Anillin-ΔPH-GFP cells treated for 3 d with LacI (control, n = 30) or Anillin dsRNAs (n = 75). Mean values are shown; data are from a single representative experiment out of three repeats. Times are given in hours, minutes, and seconds. Bars: (C and D) 5 µm; (E) 1 µm.

Sticky acts to limit extrusion and shedding and retains Anillin at the MR

Cit-K, Sticky in *Drosophila*, is a conserved Rho-associated kinase required for a late step of cytokinesis (Di Cunto et al., 2000, 2002; D'Avino et al., 2004; Echard et al., 2004; Naim et al., 2004; Shandala et al., 2004; Gruneberg et al., 2006). Human Cit-K and Anillin can be coimmunoprecipitated, and Cit-K has been suggested to maintain Anillin at the MR (Gai et al., 2011; Watanabe et al., 2013). Cit-K/Sticky and Anillin depletion phenotypes also bear some similarities, such as plasma membrane blebbing (Somma et al., 2002; Echard et al., 2004; Naim et al., 2004; Gai et al., 2011). However, because the relationship between Anillin and Cit-K/Sticky remains unclear, we reexamined Sticky depletion phenotypes. Immunoblot analysis revealed that 3-d incubation of S2 cells with Sticky dsRNAs led to a >90% depletion of both major migrating forms of Sticky (Fig. S5 A), similar to that described previously (D'Avino et al., 2004).

Time-lapse sequences captured at 1-min intervals with a 63× objective revealed that Sticky-depleted CRs closed with normal kinetics and morphology (Fig. 6, A and B; and Videos 6 and 7), consistent with previous studies (Echard et al., 2004; Bassi et al., 2011). The midbody microtubules also adopted their characteristic compacted morphology at the close of furrowing (Fig. 6, A and B), unlike Anillin-depleted cells (Fig. 3, B and D; Kechad et al., 2012). However, measuring Anillin-GFP intensities revealed that Anillin levels continued to increase after the close of furrowing, such that the peak intensity of the nascent MR was ∼10 min later than that of control cells (Fig. 6 C). At the time of normal MR formation and maturation, Anillin-GFP displayed enhanced extrusion and internalization events (Fig. 6 D). As in controls, blebs and tubules of Anillin-positive membranes formed and subsequently left the MR region by lateral movement or outright shedding (Fig. 6, A and B; and Videos 6 and 7). Although we observed clear examples of both internalization and extrusion/shedding in both control and Sticky-depleted cells, it was often difficult to differentiate between the two in any given case, especially as extruded material could subsequently be internalized. We therefore simply quantified removal (by either mechanism). This revealed that more Anillin-GFP was removed from Sticky-depleted nascent MRs and over a longer period than in controls (Fig. 6 D). Removal continued until Anillin-GFP was no longer detectable at the MR site, and furrows either regressed within a few minutes or underwent abscission prematurely (Fig. 6, A and B; and Videos 6 and 7).

To better define the outcomes of cytokinesis attempts upon Sticky depletion, we acquired time-lapse sequences at 2–4-min intervals over longer periods using a 40× objective. 77% of attempts failed, whereas 23% succeeded ($n > 65$; Fig. 6 E). Interestingly, successes occurred earlier and with much less variability than untreated controls (Fig. 6 E), confirming our earlier inference of premature abscission in Sticky-depleted cells obtained from scoring the frequency of paired S2 cells (Echard et al., 2004). These successful divisions probably represent a hypomorphic phenotype, as they were more prevalent at earlier times after dsRNA addition, with failures predominating later. Failures resulted from rapid furrow regression 77 ± 15 min (mean ± SD; $n = 50$) after CR closure (Fig. 6 E). Thus, ∼75 min after furrowing, Sticky-depleted nascent MRs either quickly resolved or regressed and failed. In both cases, a persistent Anillin-GFP–positive MR structure failed to form in >90% of division attempts ($n > 58$ per condition; Fig. 6, A and B).

Analysis of fixed cells revealed that Pnut (Fig. 6 F) and Rho1 (Fig. 6 G) were also enriched in the extruded Anillin-positive membranes, whereas F-actin was depleted (Fig. 6 H), as had been observed for extrusion in cells that were not depleted of Sticky (Fig. 2). Importantly, nascent MRs of Sticky-depleted untransfected cells also revealed markedly enhanced extrusion of endogenous Anillin compared with controls (Fig. 6, I and J), confirming that Sticky limits extrusion and that extrusion is not simply a consequence of Anillin-FP overexpression. We conclude that Sticky acts to retain Anillin at the mature MR.

Sticky acts with the N terminus of Anillin to promote both MR formation and CR stability

Sticky depletion had no effect on the recruitment or removal of Anillin-ΔN-FP (Fig. 7 A) but greatly diminished the localization of Anillin-ΔC-FP to the nascent MR (Fig. 7 B) and prevented it from forming stable MR-like structures, whether or not endogenous Anillin was codepleted (Fig. 7 C). Furthermore, a functional Sticky-mCh localized to internal Anillin-ΔC-GFP–dependent MR-like structures that resulted upon depletion of endogenous Anillin (Fig. 7 D) but did not colocalize with Anillin-ΔN-GFP–positive structures that accumulate around the nascent MR when endogenous Anillin is present (Fig. 7 E). Thus, Sticky is specifically required to retain the N terminus of Anillin at the mature MR.

Cleavage furrows are inherently unstable (Sedzinski et al., 2011) and oscillate after certain perturbations, including Anillin depletion (Straight et al., 2005; Zhao and Fang, 2005; Hickson and O'Farrell, 2008b; Piekny and Glotzer, 2008; Goldbach et al., 2010) and overexpression of full-length or truncated Cit-K (Madaule et al., 1998; Gai et al., 2011). Remarkably, cells expressing Anillin-ΔC-FP and depleted of endogenous Anillin, which furrow slowly without oscillating and form stable MR-like structures (Kechad et al., 2012), also became prone to oscillate when Sticky was codepleted (Fig. 7, F and H). This indicates that Sticky promotes the ability of the Anillin N terminus to stabilize furrows.

Because Pnut depletion blocked Anillin removal from the MR and Sticky depletion blocked Anillin retention, we tested the effects of codepleting Sticky and Pnut. Little, if any, evidence of extrusion or internalization of Anillin-GFP was observed, indicating that the enhanced extrusion observed upon Sticky depletion was still Pnut dependent (Fig. 7 G and Video 8). In 39% ($n = 46$) of cells, the formation of stable MR-like structures was abolished, as expected (Fig. 7 I). The remaining 61% exhibited an intermediate phenotype whereby Anillin-positive MR structures persisted, but unlike control or Pnut-depleted cells (Fig. S4, A and B), these often did not label for myosin (Fig. S4, C and D). This partial destabilization of the MR suggests that Sticky acts to retain myosin at the MR. Furthermore, some of the structures

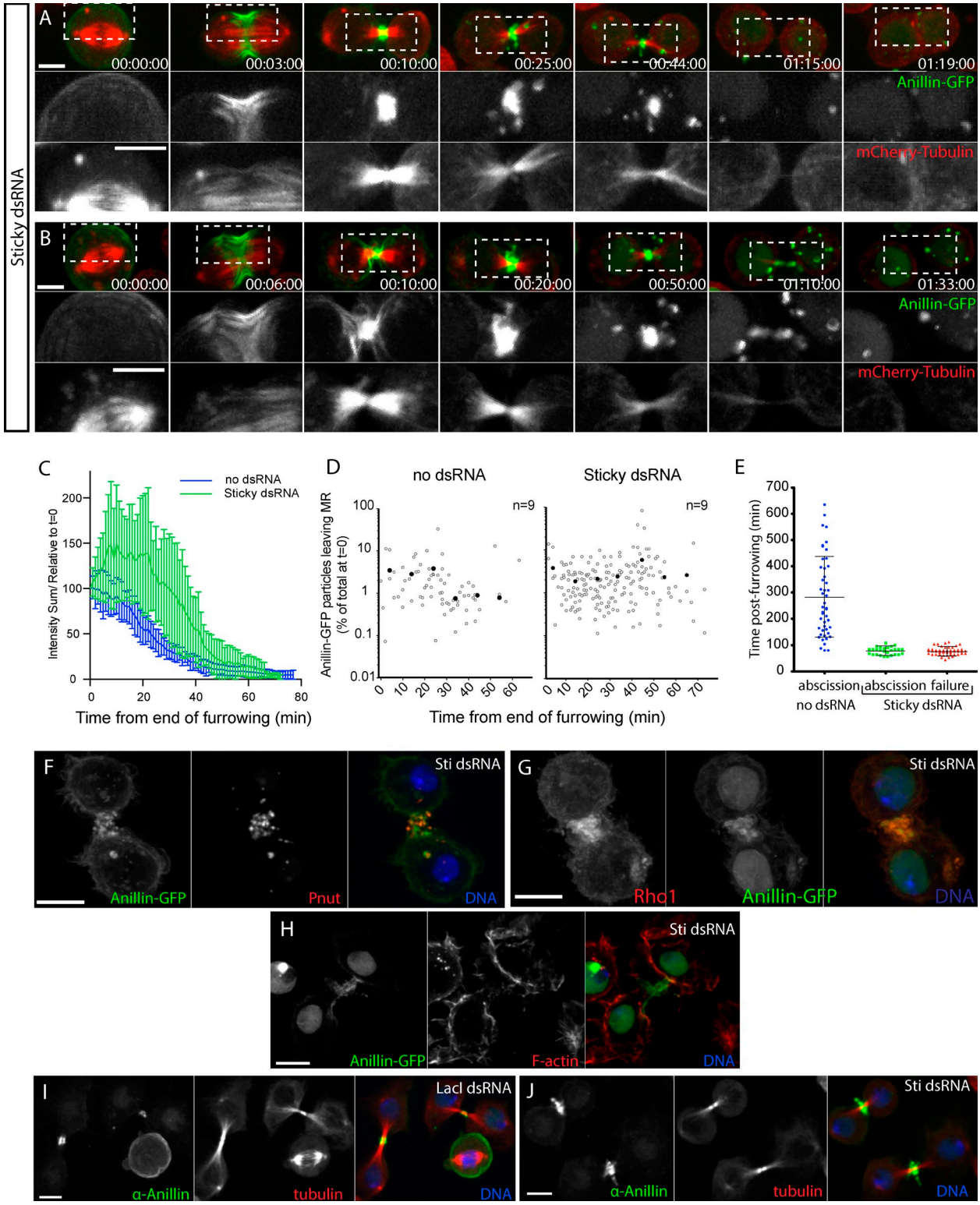

Figure 6. **Sticky acts to limit extrusion/shedding and retain Anillin at the MR.** (A and B) Sticky-depleted cells expressing Anillin-GFP and mCh-tubulin failing cytokinesis (A) or prematurely abscising (B) (63× objective). Boxed regions are shown magnified and with separated channels below. (C) Quantification of relative Anillin-GFP intensities (sum intensity) at the MR from the time of midbody formation in control (n = 9) and Sticky-depleted cells (n = 17). (D) Quantification of individual extrusion or internalization events (open circles) plotted as a function of time and associated Anillin-GFP $\log_{10}$ intensity (as a measure of total intensity at the close of furrowing, t = 0). Closed circles represent mean values for each 10-min interval (n = 9 cells each, from one experiment representative of two repeats). (E) Timing of abscission or furrow regression (failure) events of individual Anillin-GFP cells treated for 30–48 h with or without Sticky dsRNAs. Data are from two independent experiments, horizontal lines mark the mean times, and error bars show the SDs. (F–H) Confocal images of Sticky-depleted cells expressing Anillin-GFP (left), stained for Pnut (F, center), Rho1 (G, left), or F-actin (H, center) and DNA. (I and J) Confocal images of untransfected S2 cells treated with LacI control dsRNA (I) or Sticky dsRNA (J) and stained for endogenous Anillin (left), tubulin (center), and DNA (63× objective). Times are given in hours, minutes, and seconds. Bars, 5 µm. See also Videos 6 and 7.

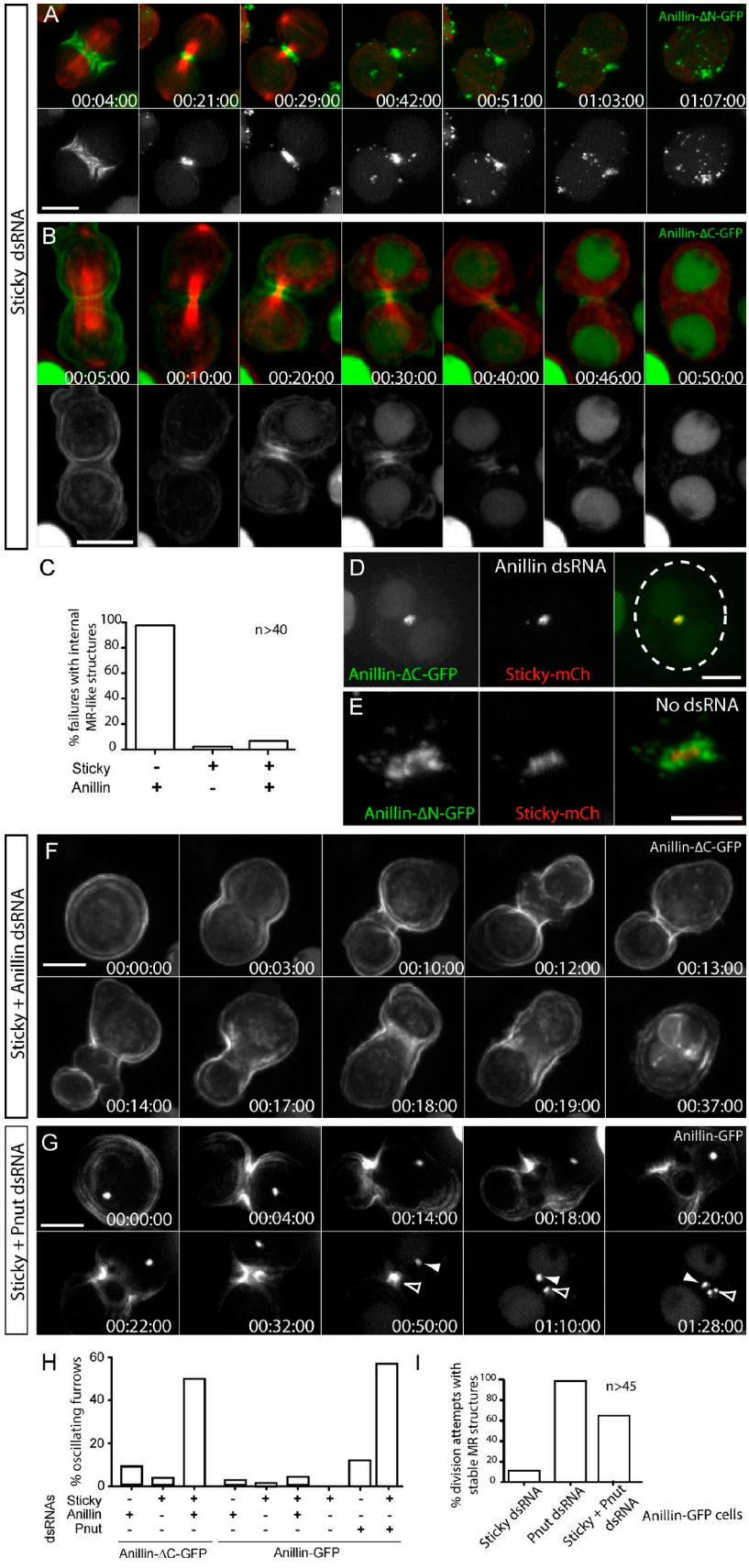

Figure 7. **Sticky acts with the N terminus of Anillin to promote both MR formation and CR stability.** (A and B) Time-lapse sequence of cells expressing mCh-tubulin and Anillin-ΔN-GFP (A) or Anillin-ΔC-GFP (B) after a ∼30-h incubation with Sticky dsRNAs (63× objective and 2 × 2 camera binning). (C) Quantification from time-lapse records of failed attempts at cytokinesis that form internal Anillin-ΔC-FP–positive MR-like structures after incubation with the indicated dsRNAs. Data are from two independent experiments. (D and E) Confocal images of cells coexpressing Sticky-mCh and Anillin-ΔC-GFP (D) or Anillin-ΔN-GFP (E) after endogenous Anillin depletion. Dotted line in D marks the cell boundary (63× objective and no camera binning). (F) Time-lapse sequence of a cell expressing Anillin-ΔC after codepletion of Sticky and Anillin. (G) Time-lapse sequence of a cell expressing Anillin-GFP after codepletion of Pnut (144–162-h RNAi) and Sticky (30–48-h RNAi), captured with a 63× objective with 2 × 2 camera binning. Closed arrowheads mark a presumed MR remnant from a previous division. Open arrowheads mark failing MR from the current division attempt. (H) Quantification from time-lapse records (40× objective and 2 × 2 camera binning) of the percentage of Anillin-GFP and Anillin-ΔC-GFP cells displaying oscillating furrows during CR closure after incubation with the indicated dsRNAs ($n > 78$ per condition from two independent experiments). (I) Quantification from time-lapse records (40× objective and 2 × 2 camera binning) of attempts at cytokinesis that result in Anillin-GFP–positive MR structures after incubation with indicated dsRNAs ($n > 45$ per condition, from two independent experiments). Times are given in hours, minutes, and seconds. Bars, 5 µm. See also Video 8.

were clearly not closed rings but had less well-defined shapes (e.g., Fig. 7 G and Video 8). Persistence of Anillin at these structures may reflect the existence of other Sticky-independent mechanisms that contribute to Anillin retention at the midbody.

Strikingly, cells codepleted of Sticky and Pnut were prone to oscillate during furrowing (53% oscillations, n = 135), whereas singly depleted cells were much less so (<10% oscillations; Fig. 7, G and H; and Video 8). During oscillations, Anillin-FP migrated laterally in repeated cycles, much like myosin does upon Anillin depletion. The fact that codepletion of Sticky and Pnut destabilized furrows and caused Anillin to oscillate suggests that Pnut contributes to a stabilizing influence of the Anillin C terminus. Anillin-ΔN-FP, comprising only the Anillin C terminus, failed to rescue oscillations but was completely disconnected from actomyosin (Kechad et al., 2012), underscoring the importance of the linkage to actomyosin. These data show that Anillin stabilizes furrows in part by linking actomyosin to the membrane-associated septin cytoskeleton and in part via a distinct Sticky-dependent action of its N terminus.

Sticky's essential role during MR formation is as a scaffold

We next wished to test whether Sticky kinase activity is required to retain Anillin-GFP at the MR. We generated inducible cell lines that coexpressed Anillin-GFP and mCh-tagged wild-type or kinase-dead (KD) versions of Sticky, at roughly endogenous levels (Fig. 8 A). Both Sticky-mCh and Sticky-KD-mCh were faithfully recruited to the CR and MR, although both also led to the formation of Anillin-GFP–negative, intracellular aggregates, similar to those described by others (Fig. 8, C and D; and Videos 9 and 10; Eda et al., 2001). Expression of either Sticky-mCh or Sticky-KD-mCh rescued the widespread failures of cytokinesis induced by depletion of endogenous Sticky using a dsRNA directed against the Sticky 3′ UTR (Fig. 8 B). That formation of Sticky- and Anillin-positive MRs (Fig. 8, C–E; and Video 10) were rescued in Sticky-KD-mCh cells indicates that Sticky kinase activity is dispensable for both MR formation and abscission (Fig. 8, B and E). However, abscission timing was slightly accelerated for Sticky-KD-mCh MRs (128 ± 49 min, mean ± SD; n = 28) than for Sticky-mCh MRs (196 ± 67 min, mean ± SD; n = 26). Furthermore, the majority of cells that failed did not recruit detectable levels of Sticky-mCh (7/8 failures) or Sticky-KD-mCh (18/24 failures) to the CR/MR, consistent with failures reflecting the lack of Sticky rather than the lack of kinase function (Fig. 8 B and Fig. S3 B). In addition, excess Sticky-mCh and Sticky-KD-mCh were both also internalized and extruded/shed with Anillin-GFP (Fig. 8, C–E; and Videos 9 and 10), indicating that Sticky must itself be subject to retention at the midbody. We conclude that the essential role of Sticky in these cells is as a scaffold that serves to retain Anillin and stabilize the MR.

Discussion

The organization of the cell cortex during closure of the CR and formation of a stable MR remains poorly defined. We show in *Drosophila* S2 cells that the late CR/nascent MR thins via a maturation process that lasts ∼1 h and that involves a molecular tug of war between stable retention and dynamic removal of the membrane- and cytoskeleton-associated scaffold Anillin. Retention requires a scaffold function of the Cit-K Sticky and the N terminus of Anillin, whereas removal requires septins and the C terminus of Anillin and includes dramatic extrusion and shedding of membranes. Simultaneous perturbation of these antagonistic processes disrupts not only MR maturation but also CR stability, supporting our previous proposal that the CR and MR represent different stages of the same structure (Kechad et al., 2012). The work provides novel insight into the elusive mechanisms of CR closure and its maturation to the MR (Fig. 9).

Anillin-septin–dependent membrane removal

The extrusion and shedding of membrane from the nascent MR was unexpected; however, it is highly reminiscent of Anillin- and prominin-1–positive, membrane-bound particles that shed from apical MRs in the vertebrate neuroepithelium (Dubreuil et al., 2007). EM has also revealed budding of membranous structures from the MR of human D98S cells (Mullins and Biesele, 1977) and prominent membrane microvilli in cleavage stage sea urchin embryos (Schroeder, 1972). We have also observed extrusion of Anillin from the nascent MRs of human HeLa and neuroblastoma cells (unpublished data). Finally, we note that tubules of Anillin- and Pnut-positive membranes are shed from the newly formed cells at the close of cellularization of the *Drosophila* embryo, a process mechanistically related to cytokinesis (unpublished data; Adam et al., 2000; Field et al., 2005). Thus, membrane extrusion may be a universal feature of animal cell cytokinesis.

Is membrane removal the cause or consequence of CR closure?

Key questions arise concerning the mechanism of Anillin-septin membrane extrusion and whether it is a cause or consequence of CR closure or both. In mammalian interphase cells, membrane blebs recruit septins, after F-actin, to facilitate bleb retraction (Gilden et al., 2012). However, the membrane protrusions/tubules that we describe are enriched in Anillin from their first emergence, they are poor in actin and they never retract. Thus, rather than being recruited to or trapped in preexisting blebs, we favor the model that Anillin directs septin-dependent membrane tubulation. Septins are capable of tubulating membranes (Tanaka-Takiguchi et al., 2009), although the topology of such structures is reversed compared with the extrusions that we describe. However, it remains unclear how Rho1 and Anillin (and potentially other cytokinesis proteins) might alter septin behaviors. Experimentally disconnecting the N terminus of Anillin from the actomyosin network, either by deleting the N terminus of Anillin (Kechad et al., 2012) or by disrupting the actin cytoskeleton with Latrunculin A (Hickson and O'Farrell, 2008b), triggers the C terminus of Anillin to induce Pnut-dependent remodeling of the plasma membrane, resulting in either punctate or tubular protrusions that extend outwards from the cell. These

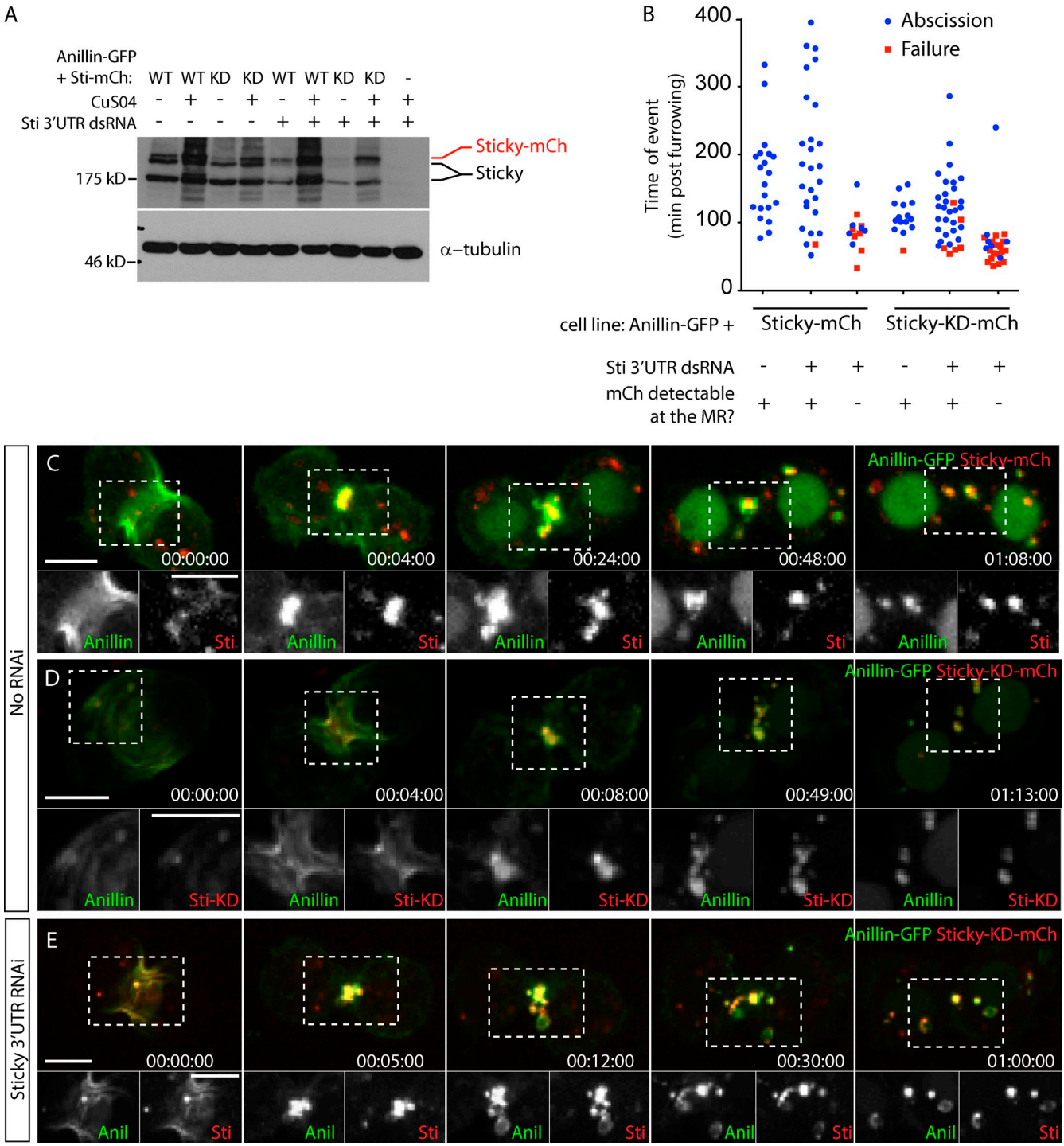

Figure 8. **Sticky's essential role during MR formation is as a scaffold.** (A) Anti-Sticky (Sti) immunoblot of cell lysates from indicated cell lines after Sticky 3′ UTR dsRNA or LacI control dsRNA incubation, with anti-tubulin blot as a loading control. WT, wild type. (B) Timing of abscission or furrow regression (failure) of cells coexpressing Anillin-GFP and Sticky-mCh or Sticky-KD-mCh, treated for 3–5 d with or without Sticky 3′ UTR dsRNAs. Data are from two independent experiments. (C and D) Time-lapse sequence of a cell coexpressing Anillin-GFP and Sticky-mCh (C) or Sticky-KD-mCh (D). Separated channels of the boxed regions are shown magnified at the bottom. (E) Time-lapse sequence of a cell coexpressing Anillin (Anil)-GFP and Sticky-KD-mCh after depletion of endogenous Sticky. Times are given in hours, minutes, and seconds. Bars, 5 µm. See also Videos 9 and 10.

data argue that the extrusions at the late CR/nascent MR may simply reflect the local disassembly of actin, thereby liberating Anillin N termini and allowing Anillin C termini/septins to tubulate membranes in such a dramatic fashion. Indeed, membrane extrusion is most obvious at the time when the MR is becoming resistant to Latrunculin A (Echard et al., 2004), suggesting coordination with disassembly of the actin ring. Finally, actin and Anillin-ΔC were notably absent from the extruded and shed membranes, indicating that not all CR components are removed in this way.

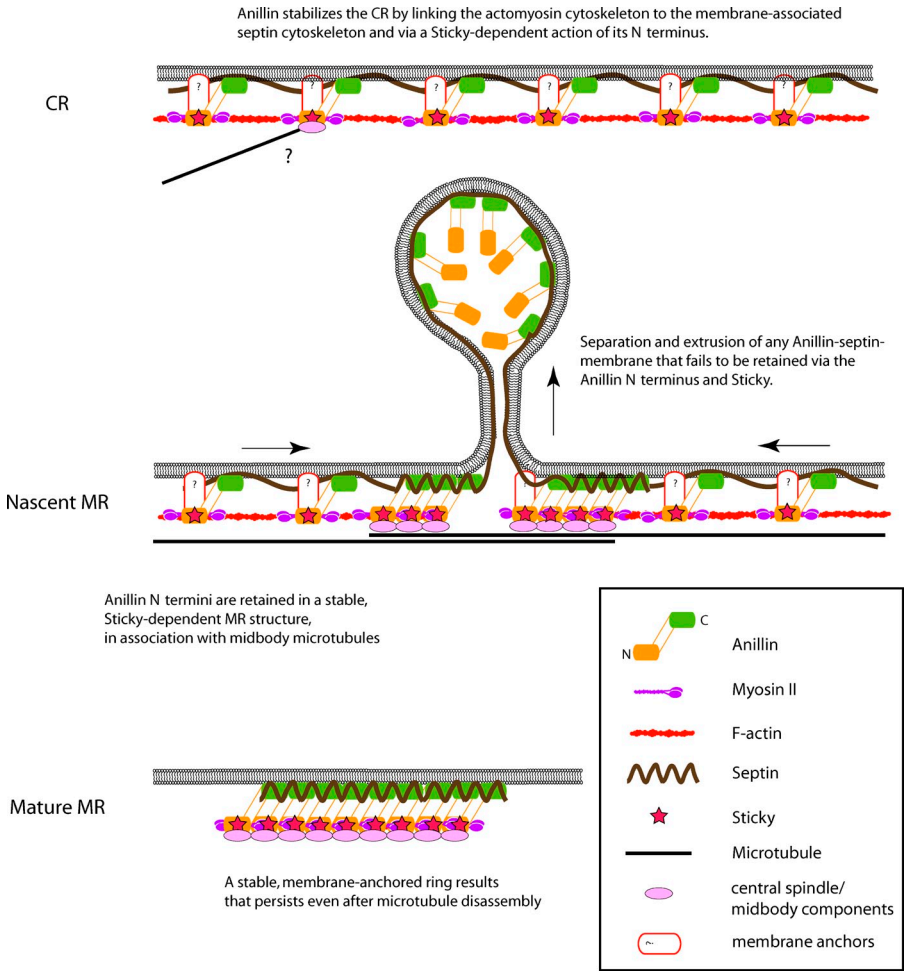

Figure 9. **Model for the maturation of the CR and MR.** (top) At the CR stage, Anillin links the plasma membrane–associated septin cytoskeleton to actomyosin, stabilizing the furrow. Anillin also stabilizes the furrow via a separate Sticky-dependent action of its N terminus. (middle) At the nascent MR, Sticky, myosin, and the Anillin N terminus are retained at the midbody, where they will form a mature MR structure. Septins act on the C terminus of Anillin to remove membrane-associated Anillin molecules, whose N termini are liberated upon disassembly of the F-actin ring. Note that this removal does not only occur at the center of the midbody as depicted. (bottom) Septins and the C termini of Anillin molecules that are retained also act as membrane anchors for the mature MR that persists beyond ~1 h after furrowing.

Can furrow oscillations result from impeding CR disassembly?

The CR closes by disassembly (Schroeder, 1972; Carvalho et al., 2009). Our results suggest that this involves both depolymerization and membrane-associated removal. Accordingly, Anillin and septins may sequester the excess membrane that is liberated upon actomyosin depolymerization. Anillin-depleted CRs fail to close to completion and become unstable and oscillate (Straight et al., 2005; Zhao and Fang, 2005; Hickson and O'Farrell, 2008b; Piekny and Glotzer, 2008; Goldbach et al., 2010). Our findings raise the possibility that this phenotype reflects a failure to sequester membrane (via septins) that impedes the normal disassembly of the actin ring, combined with the loss of an additional Sticky-dependent scaffolding role of the N terminus of Anillin.

We note that Sticky and Pnut codepletion did not completely phenocopy Anillin depletion. The latter is more severe with a proportion of cells that undergo wild oscillations that are too unstable to allow ingression beyond 50% closure (Kechad et al., 2012). Sticky- and Pnut-codepleted cells, although they oscillated, mostly ingressed to completion and then failed at the MR stage (this study). Thus, Anillin likely has additional inputs into furrow stability that are independent of Sticky and Pnut. RacGAP50C/Tum is a strong candidate known to interact with the AHD (D'Avino et al., 2008; Gregory et al., 2008).

The essential role of Sticky is as a scaffold for the mature MR, but it also functions during furrowing

We show that Sticky is required to retain the N terminus of Anillin at the mature MR. Human Cit-K can phosphorylate the MRLC (Yamashiro et al., 2003), and MRLC is another component of the MR in S2 cells (Dean and Spudich, 2006; Kechad et al., 2012). Expression of phosphomimetic MRLC (Spaghetti squash–E20E21) in S2 cells cannot rescue for Sticky depletion, indicating that myosin phosphorylation cannot be the only essential role of Sticky (Dean and Spudich, 2006). Our results further show that kinase activity is completely dispensable for the essential function of Sticky because a KD version is still able to form a stable MR and rescue cytokinesis. In agreement with this, the central coiled-coil region of human Cit-K is sufficient to support cytokinesis in HeLa cells (Watanabe et al., 2013). The fact that Sticky was extruded and shed with Anillin suggests that Sticky itself must be retained by additional, saturable mechanisms at the midbody, likely via KIF14-dependent mechanisms (Gruneberg et al., 2006; Bassi et al., 2013; Watanabe et al., 2013).

Although Cit-K/Sticky localizes to the CR (Madaule et al., 1998; Eda et al., 2001; D'Avino et al., 2004; Bassi et al., 2011), whether it acts there is a long-standing enigma. Our findings confirm that it does, albeit redundantly. First, unlike control furrows,

Sticky-depleted furrows continued to accumulate Anillin-GFP for 10 min after closure, indicating that Sticky normally functions at this time. Second, Sticky depletion caused furrow oscillations in cells codepleted of Pnut or in cells expressing Anillin-ΔC and codepleted of endogenous Anillin. This indicates that Sticky plays a role in furrow stability that is redundant with the C terminus of Anillin and Pnut. We attempted to test whether kinase activity was required for this role. However, rescuing Sticky depletion in the context of Pnut codepletion was problematic. The longer induction times required by the fact that Pnut depletion takes many days resulted in poor recruitment of Sticky-mCh and Sticky-KD-mCh to CRs, with both proteins preferring to form ectopic aggregates. Thus, although kinase activity is dispensable for Sticky's essential role at the MR, it remains possible that its kinase activity contributes to CR stability.

Concluding remarks

Current models for CR closure focus on the cytoskeletal proteins and pay little attention to the plasma membrane to which these elements are anchored. Although net membrane addition may be required during furrow ingression (Albertson et al., 2005; McKay and Burgess, 2011; Neto et al., 2011), our findings highlight a need for membrane removal from the furrow apex that must be coordinated with CR disassembly and MR assembly. Extrusion and shedding is one way of achieving this; other potential mechanisms include internalization and lateral outflow within the lipid bilayer. Theoretical and experimental analyses in different systems will be needed to fully test this novel perspective.

Materials and methods

Constructs, cell lines, and RNAi

All constructs were generated by PCR amplification of the ORF, without stop codons, followed by cloning into pENTR-D-TOPO (Invitrogen) followed by recombination using LR Clonase into appropriate destination vectors (Drosophila Gateway Vector Collection; T. Murphy, Carnegie Institution for Science, Washington, DC). Anillin-GFP (pMT-WG, driven by the metallothionein promoter), Anillin-mCh (pAc-WCh, driven by the constitutive *Act05C* promoter), mCh-tubulin (pAc-ChW), $MRLC^{Sqh}$-GFP (endogenous *spaghetti squash* promoter), Anillin-ΔC-FP (pMT-WG or pMT-WCh), Anillin-ΔN-FP (pMT-WG or pMT-WCh), and Pavarotti-GFP (pMT-WG) have been described previously (Echard et al., 2004; Hickson and O'Farrell, 2008b; Kechad et al., 2012). Internal deletions and site-directed mutagenesis were performed by PCR by overlap extension followed by cloning into pENTR-D-TOPO and subsequent recombination into pMT-WG and pMT-WCh. All Anillin constructs derive from clone LD23793 (Berkeley Drosophila Genome Project Gold collection; Drosophila Genomics Resource Center) that encodes the CG2092-RB polypeptide. Note that CG2092-RB has an additional 27 residues within the actin-binding domain that is absent in CG2092-RA (Field and Alberts, 1995), but CG2092-RB is better supported by sequencing data. Anillin-ΔN+CD-FP encodes amino acids 410–1,239 and lacks all N-terminal domains up to and including the ActBD. Anillin-ΔPH-FP encodes amino acids 1–1,104 and thus lacks the last 135 residues comprising the entire PHD. Anillin-ΔActBD encodes amino acids 1–255 and 410–1,239 and lacks the minimal ActBD defined in Field and Alberts (1995). Anillin-ΔMyoBD encodes amino acids 1–145 and 238–1,239 and lacks 92 amino acids homologous to the *Xenopus* MyoBD defined in Straight et al. (2005). The *sticky* (CG10522) ORF was PCR amplified from clone RE26327 (Drosophila Gene Collection release 2 collection; Drosophila Genomics Resource Center). The Sticky KD mutant was generated by site-directed mutagenesis using primers 5′-GACATATACGCCATGGCGGCGATCAAAAAGTCGGTG-3′ and 5′-CACCGACTTTTTGATCGCCGCCATGGCGTATATGTC-3′, which introduced K142A and K143A mutations in the kinase domain. The Aurora B ORF was amplified by RT-PCR from S2 cell cDNA and was described in Smurnyy et al. (2010). Myrpalm-GFP (in pAc-WG) was a gift from S. Carreno (Institut de Recherche en Immunologie et Cancérologie, Université de Montréal, Montréal, Quebec, Canada) and encodes the first 16 amino acids of Lyn (MGCIKSKRKDNLNDDE), including myristoylation and palmitoylation signals, upstream of GFP and driven by the *act05C* promoter. LifeAct-GFP encodes the 17-amino sequence described by Riedl et al. (2008) cloned upstream of GFP (pMT-WG). The Dendra2 sequence was subcloned from pDendra2-N1 (Takara Bio Inc.) into pAc-WG, replacing GFP, to generate pAc-WD2 and allowing subsequent generation of Anillin-Dendra2 by Gateway recombination. All constructs were verified by sequencing.

Plasmids were used to transfect *Drosophila* Schneider's S2 cells using Cellfectin reagent (Invitrogen), together with pCoHygro and additional plasmids as needed to generate stable, hygromycin-resistant cell lines following established protocols (Invitrogen). After selection, cells were cultured in Schneider's medium supplemented with 10% fetal calf serum (Invitrogen) and penicillin/streptomycin.

dsRNAs were generated using in vitro transcription kits (RiboMAX; Promega), and DNA templates were generated in a two-step PCR amplification from cDNA or genomic DNA, as described previously (Echard et al., 2004). In brief, in the first round PCR, gene-specific primer sequences included a 5′ anchor sequence (5′-GGGCGGGT-3′), whereas the second round PCR used a universal T7 anchor primer (5′-TAATACGACTCACTATAGGGAGACCACGGGCGGGT-3′). Gene-specific primer sequences were previously described for *anillin* dsRNA (Echard et al., 2004; Hickson and O'Farrell, 2008b), *anillin* 3′ UTR dsRNA (Hickson and O'Farrell, 2008b), *pnut* dsRNA (Hickson and O'Farrell, 2008b), and *sticky* dsRNAs (Echard et al., 2004). *shrub/CHMP4/CG8055* and *dIST1/CG10103* dsRNAs were generated using primer pairs 5′-GGGCGGGTTCGATACAAAGCTAAGACTGCG-3′ and 5′-GGGCGGGTATGATCCAGACATGAAGAGCAGC-3′ (Shrub) and 5′-GGGCGGGTGTTGGTGTTCAGATCCTTCTCC-3′ and 5′-GGGCGGGTCTACAGAGCGATATAGCCGAGC-3′ (dIST1). The *sticky* 3′ UTR dsRNA was generated using primer sequences 5′-GGGCGGGTGCATATAGATGAAGGATATAT-3′ and 5′-GGGCGGGTTTTAAAATATTATGCGACTTC-3′.

RNAi experiments were performed as follows: cells were plated in 96-well dishes and incubated with ∼1 µg/ml dsRNA. 12–24 h before imaging or fixation, cells were transferred to 8-well chambered coverglass dishes (Lab-Tek; Thermo Fisher Scientific). Live imaging was performed between 30 and 72 h for Anillin dsRNAs, between 30 and 48 h for Sticky dsRNAs, and between 144 and 192 h for Pnut dsRNA, in which case cells were split and fresh dsRNA added on the fourth day. These dsRNA incubation times were maintained for codepletion experiments, but the individual dsRNA incubations were performed in the presence of irrelevant LacI control dsRNAs to control for possible effects of combining dsRNAs.

Live-cell microscopy

Live-cell imaging of *Drosophila* S2 cells in Schneider's medium was performed at room temperature using a spinning-disc confocal system (UltraVIEW Vox; PerkinElmer) using a scanning unit (CSU-X1; Yokogawa Corporation of America) and a charge-coupled device camera (ORCA-R2; Hamamatsu Photonics) fitted to an inverted microscope (DMI6000 B; Leica) equipped with a motorized piezoelectric stage (Applied Scientific Instrumentation). Image acquisition was performed using Volocity versions 5 and 6 (PerkinElmer). Routine and long-time course imaging was performed using a Plan Apochromat 40×, 0.85 NA air objective with camera binning set to 2 × 2, high-resolution imaging was performed using Plan Apochromat 63 or 100× oil immersion objectives, NA 1.4, with camera binning set to 2 × 2 unless otherwise described in the figure legends.

Expressions of FP fusions under the control of the metallothionein promoter (pMT plasmids) were induced with 250 µM $CuSO_4$ at the time of dsRNA addition in the case of rescue experiments, or when cells were transferred to imaging dishes, 12–24 h before the start of imaging. Where described, MG132 (Enzo Life Sciences) was added to a final concentration of 5 µM directly to the culture medium.

Immunofluorescence microscopy

Cells were transferred to either 8-well chambered coverglass dishes (Lab-Tek) or 96-well glass-bottomed plates (Whatman) ≥2 h before fixation for 5 min in 4% formaldehyde/0.1% glutaraldehyde in PBS. After permeabilization and blocking in PBS containing 0.1% Triton X-100 (PTX buffer) and 5% normal goat serum, cells were incubated with primary antibodies (rabbit anti-Anillin, a gift from C. Field, Harvard Medical School, Boston, MA, used at 1:1,000; and concentrated mAb 4C9H4 anti-Pnut, obtained from Developmental Studies Hybridoma Bank, used at 1:400) at 4°C overnight, washed with PTX buffer, and incubated for 1 h with Alexa Fluor 488–, Alexa Fluor 546–, or Alexa Fluor 647–conjugated goat anti–mouse or

anti–rabbit secondary antibodies (1:500; Molecular Probes/Invitrogen), as appropriate. Where appropriate, Hoechst 33258 (1:500) and rhodamine-phalloidin (1:500; Molecular Probes) were added at the same time. Cells were washed in PTX and mounted in Fluoromount-G (SouthernBiotech). Images were acquired using the UltraVIEW Vox system described in the previous section using oil immersion Plan Apochromat 63 or 100×, 1.4 NA objectives.

FRAP and image analysis

FRAP was performed using the PhotoKinesis module (PerkinElmer) controlled through Volocity software. 5-µm-thick stacks of four z sections were acquired with a 63× objective and 2 × 2 camera binning. Acquisition was at maximum speed (exposure time of 200 ms) for the first 15 s after bleaching (representing cytoplasmic recovery) and then at one image per 15 s for 5 min. Percent recovery = percentage (maximum intensity after bleach − intensity at bleach)/(intensity before bleach − intensity at bleach). All intensity values in FRAP experiments were normalized to the first time point of acquisition. For statistical analysis, an unpaired *t* test was performed using Prism (GraphPad Software).

MR volume measurements were obtained as follows: cells were imaged using a 63×, 1.4 NA objective (12 z sections at 1-min intervals) during ≥1 h after furrowing using Volocity acquisition. Datasets were then exported as Openlab LIFF files (PerkinElmer) and analyzed using Imaris 7 quantification module (Bitplane) as follows: a surface around the MR was selected using intensity threshold, and the volume of this surface was determined empirically for each MR. These values were then expressed as percentages relative to the value of MR volume at the end of furrowing (the first time point of analysis). Relative fold differences in MR volume were calculated relative to the volume of control Anillin-GFP MRs for each given time point after furrowing. The same process was applied for intensity measurements of each extrusion, internalization, or shedding (Fig. 6 D).

Intensity measurements of MRs were performed using the Volocity select objects by percent intensity tool. Optimal percentage values were determined empirically for each MR, and the resulting sum intensity values were then expressed as percentages relative to the highest value within the given time series (usually, t = 0). Datasets were background corrected. Quantification of the Anillin-GFP loss in Fig. 6 C was performed using Imaris 7 after export from Volocity as Openlab LIFF files. Individual shedding events were selected by creating surfaces using variable thresholds between different cells. Intensity values of individual shedding events were expressed as percentages relative to the total intensity associated with the MR at the start of the given time series. Images were processed for publication using Photoshop CS (Adobe) and assembled as figures using Illustrator CS (Adobe). Video files were exported from Volocity as QuickTime videos (Apple).

Immunoblotting

S2 cells were grown in 12-well dishes, treated with the indicated dsRNAs, and harvested by centrifugation. Cells were lysed in lysis buffer (50 mM Tris-HCl, pH 7.5, 150 mM NaCl, and 1% Triton X-100 completed with protease inhibitor cocktail [Roche]), and total cell lysates were subjected to SDS-PAGE (8–15% polyacrylamide). Proteins were transferred to a nitrocellulose membrane and blocked with 5% milk in TBS containing 0.2% Tween 20 (TBST). The membrane was cut at the appropriate molecular weight marker with the upper molecular weight part immunoblotted with affinity-purified anti-Anillin antibodies (1:1,000; generated in rabbits against amino acids 1–409 of Anillin fused to GST; a gift from J. Brill, The Hospital for Sick Children [SickKids], Toronto, Ontario, Canada; Goldbach et al., 2010) or anti-Sticky antiserum (1:3,000, generated in rabbits against a fragment of the Sticky protein [amino acids 531–742] fused to a C-terminal 6×His tag, a gift from P. D'Avino, Cambridge University, Cambridge, England, UK; D'Avino et al., 2004), whereas the lower molecular weight part was blotted with mAb anti-tubulin antibody (clone DM1A; 1:1,000; Sigma-Aldrich). For anti-Pnut (1:1,000; concentrated supernatant from clone 4C9H4; Developmental Studies Hybridoma Bank; Neufeld and Rubin, 1994), immunoblotting was performed in duplicate in which one membrane was immunoblotted with anti-Pnut and the other with mAb anti-tubulin (as indicated in this paragraph). The blots were washed in TBST, incubated with horseradish peroxidase–coupled donkey anti–rabbit or anti–mouse secondary antibodies (1:5,000; GE Healthcare), and washed again before detection of signals using Western ECL substrate (Clarity; Bio-Rad Laboratories).

EM

Drosophila S2 cells were gently pelleted by centrifugation, incubated for an hour at room temperature in a fixative consisting of 2.5% glutaraldehyde, 4% paraformaldehyde, and 5 mM $CaCl_2$ in 0.1 M cacodylate buffer, pH 7.4 (Caco), and in 1% OsO_4 in Caco for postfixation. The pellet was stained in 2% uranyl acetate overnight at 4°C, dehydrated in a graded series of ethanol, and embedded in Epon 812. Ultrathin tissue sections were cut using an ultramicrotome (Ultracut; Reichert) and mounted on copper grids. Ultrathin sections were stained with uranyl acetate and lead citrate and examined with an electron microscope (CM100; Philips).

Online supplemental material

Fig. S1 shows Anillin immunoblots demonstrating efficacy of RNAi and level of Anillin-GFP overexpression as well as additional images of membrane morphology at the nascent MR. Fig. S2 shows additional cells treated with Shrub/CHMP4 dsRNAs or MG132. Fig. S3 show behaviors of additional Anillin truncations during MR maturation. Fig. S4 shows the effects of codepletion of Sticky and Pnut on MR formation. Fig. S5 shows a Sticky immunoblot demonstrating efficacy of RNAi as well as images of Sticky-KD-mCh cytokinesis failure. Video 1 shows extrusion of Anillin-GFP from the nascent MR. Video 2 shows internalization of Anillin-GFP from the nascent MR. Video 3 shows the behavior of coexpressed Anillin-mCh and LifeAct-GFP at the nascent MR. Video 4 shows cells expressing Anillin-GFP undergoing cytokinesis after depletion of Shrub/CHMP4B. Video 5 shows a cell expressing Anillin-ΔN+CD-mCh and Anillin-ΔC-GFP undergoing cytokinesis. Video 6 shows a Sticky-depleted Anillin-GFP–expressing cell undergoing premature abscission. Video 7 shows a Sticky-depleted Anillin-GFP–expressing cell failing cytokinesis. Video 8 shows an Anillin-GFP–expressing cell codepleted of Sticky and Pnut attempting cytokinesis. Video 9 shows a cell expressing Anillin-GFP and Sticky-mCh undergoing cytokinesis after endogenous Sticky depletion. Video 10 shows a cell expressing Anillin-GFP and Sticky-KD-mCh undergoing cytokinesis after endogenous Sticky depletion. Online supplemental material is available at http://www.jcb.org/cgi/content/full/jcb.201305053/DC1. Additional data are available in the JCB DataViewer at http://dx.doi.org/10.1083/jcb.201305053.dv.

We thank Patrick O'Farrell, in whose laboratory this work was initiated (supported by National Institutes of Health grant R01-GM037193) and for comments on an early version of the manuscript. We thank Christine Field, Julie Brill, Paolo D'Avino, and the Developmental Studies Hybridoma Bank for antibodies, Ron Vale, Sébastien Carreno, and Yvonne Ruella for constructs, Raphaëlle Cadenas for generating ESCRT-III dsRNAs, and Diane Gingras for help with EM.

G.R.X. Hickson thanks the Fonds de Recherche du Québec–Santé (FRQS) for a Junior 1 scholarship. A. Kechad thanks the Fondation du Centre Hospitalier Universitaire Sainte-Justine/Fondation des Étoiles and the FRQS for graduate fellowships. This work was supported by grants from the Canadian Institutes of Health Research (MOP-97788), the Canadian Fund for Innovation, and the FRQS to G.R.X. Hickson.

Submitted: 10 May 2013
Accepted: 27 September 2013

References

Adam, J.C., J.R. Pringle, and M. Peifer. 2000. Evidence for functional differentiation among *Drosophila* septins in cytokinesis and cellularization. *Mol. Biol. Cell.* 11:3123–3135. http://dx.doi.org/10.1091/mbc.11.9.3123

Agromayor, M., J.G. Carlton, J.P. Phelan, D.R. Matthews, L.M. Carlin, S. Ameer-Beg, K. Bowers, and J. Martin-Serrano. 2009. Essential role of hIST1 in cytokinesis. *Mol. Biol. Cell.* 20:1374–1387. http://dx.doi.org/10.1091/mbc.E08-05-0474

Albertson, R., B. Riggs, and W. Sullivan. 2005. Membrane traffic: a driving force in cytokinesis. *Trends Cell Biol.* 15:92–101. http://dx.doi.org/10.1016/j.tcb.2004.12.008

Barr, F.A., and U. Gruneberg. 2007. Cytokinesis: placing and making the final cut. *Cell.* 131:847–860. http://dx.doi.org/10.1016/j.cell.2007.11.011

Bassi, Z.I., K.J. Verbrugghe, L. Capalbo, S. Gregory, E. Montembault, D.M. Glover, and P.P. D'Avino. 2011. Sticky/Citron kinase maintains proper RhoA localization at the cleavage site during cytokinesis. *J. Cell Biol.* 195:595–603. http://dx.doi.org/10.1083/jcb.201105136

Bassi, Z.I., M. Audusseau, M.G. Riparbelli, G. Callaini, and P.P. D'Avino. 2013. Citron kinase controls a molecular network required for midbody formation in cytokinesis. *Proc. Natl. Acad. Sci. USA.* 110:9782–9787. http://dx.doi.org/10.1073/pnas.1301328110

Bement, W.M., H.A. Benink, and G. von Dassow. 2005. A microtubule-dependent zone of active RhoA during cleavage plane specification. *J. Cell Biol.* 170:91–101. http://dx.doi.org/10.1083/jcb.200501131

Carlton, J.G., A. Caballe, M. Agromayor, M. Kloc, and J. Martin-Serrano. 2012. ESCRT-III governs the Aurora B-mediated abscission checkpoint

through CHMP4C. *Science*. 336:220–225. http://dx.doi.org/10.1126/science.1217180

Carvalho, A., A. Desai, and K. Oegema. 2009. Structural memory in the contractile ring makes the duration of cytokinesis independent of cell size. *Cell*. 137:926–937. http://dx.doi.org/10.1016/j.cell.2009.03.021

D'Avino, P.P. 2009. How to scaffold the contractile ring for a safe cytokinesis - lessons from Anillin-related proteins. *J. Cell Sci.* 122:1071–1079. http://dx.doi.org/10.1242/jcs.034785

D'Avino, P.P., M.S. Savoian, and D.M. Glover. 2004. Mutations in *sticky* lead to defective organization of the contractile ring during cytokinesis and are enhanced by *Rho* and suppressed by *Rac*. *J. Cell Biol.* 166:61–71. http://dx.doi.org/10.1083/jcb.200402157

D'Avino, P.P., T. Takeda, L. Capalbo, W. Zhang, K.S. Lilley, E.D. Laue, and D.M. Glover. 2008. Interaction between Anillin and RacGAP50C connects the actomyosin contractile ring with spindle microtubules at the cell division site. *J. Cell Sci.* 121:1151–1158. http://dx.doi.org/10.1242/jcs.026716

Dean, S.O., and J.A. Spudich. 2006. Rho kinase's role in myosin recruitment to the equatorial cortex of mitotic *Drosophila* S2 cells is for myosin regulatory light chain phosphorylation. *PLoS ONE*. 1:e131. http://dx.doi.org/10.1371/journal.pone.0000131

Di Cunto, F., S. Imarisio, E. Hirsch, V. Broccoli, A. Bulfone, A. Migheli, C. Atzori, E. Turco, R. Triolo, G.P. Dotto, et al. 2000. Defective neurogenesis in citron kinase knockout mice by altered cytokinesis and massive apoptosis. *Neuron*. 28:115–127. http://dx.doi.org/10.1016/S0896-6273(00)00090-8

Di Cunto, F.D., S. Imarisio, P. Camera, C. Boitani, F. Altruda, and L. Silengo. 2002. Essential role of citron kinase in cytokinesis of spermatogenic precursors. *J. Cell Sci.* 115:4819–4826. http://dx.doi.org/10.1242/jcs.00163

Dorn, J.F., and A.S. Maddox. 2011. Cytokinesis: cells go back and forth about division. *Curr. Biol.* 21:R848–R850. http://dx.doi.org/10.1016/j.cub.2011.09.012

Dubreuil, V., A.M. Marzesco, D. Corbeil, W.B. Huttner, and M. Wilsch-Bräuninger. 2007. Midbody and primary cilium of neural progenitors release extracellular membrane particles enriched in the stem cell marker prominin-1. *J. Cell Biol.* 176:483–495. http://dx.doi.org/10.1083/jcb.200608137

Echard, A., G.R. Hickson, E. Foley, and P.H. O'Farrell. 2004. Terminal cytokinesis events uncovered after an RNAi screen. *Curr. Biol.* 14:1685–1693. http://dx.doi.org/10.1016/j.cub.2004.08.063

Eda, M., S. Yonemura, T. Kato, N. Watanabe, T. Ishizaki, P. Madaule, and S. Narumiya. 2001. Rho-dependent transfer of Citron-kinase to the cleavage furrow of dividing cells. *J. Cell Sci.* 114:3273–3284.

Eggert, U.S., T.J. Mitchison, and C.M. Field. 2006. Animal cytokinesis: from parts list to mechanisms. *Annu. Rev. Biochem.* 75:543–566. http://dx.doi.org/10.1146/annurev.biochem.74.082803.133425

Elia, N., R. Sougrat, T.A. Spurlin, J.H. Hurley, and J. Lippincott-Schwartz. 2011. Dynamics of endosomal sorting complex required for transport (ESCRT) machinery during cytokinesis and its role in abscission. *Proc. Natl. Acad. Sci. USA*. 108:4846–4851. http://dx.doi.org/10.1073/pnas.1102714108

Field, C.M., and B.M. Alberts. 1995. Anillin, a contractile ring protein that cycles from the nucleus to the cell cortex. *J. Cell Biol.* 131:165–178. http://dx.doi.org/10.1083/jcb.131.1.165

Field, C.M., M. Coughlin, S. Doberstein, T. Marty, and W. Sullivan. 2005. Characterization of anillin mutants reveals essential roles in septin localization and plasma membrane integrity. *Development*. 132:2849–2860. http://dx.doi.org/10.1242/dev.01843

Gai, M., P. Camera, A. Dema, F. Bianchi, G. Berto, E. Scarpa, G. Germena, and F. Di Cunto. 2011. Citron kinase controls abscission through RhoA and anillin. *Mol. Biol. Cell*. 22:3768–3778. http://dx.doi.org/10.1091/mbc.E10-12-0952

Gilden, J.K., S. Peck, Y.C. Chen, and M.F. Krummel. 2012. The septin cytoskeleton facilitates membrane retraction during motility and blebbing. *J. Cell Biol.* 196:103–114. http://dx.doi.org/10.1083/jcb.201105127

Glotzer, M. 2005. The molecular requirements for cytokinesis. *Science*. 307:1735–1739. http://dx.doi.org/10.1126/science.1096896

Goldbach, P., R. Wong, N. Beise, R. Sarpal, W.S. Trimble, and J.A. Brill. 2010. Stabilization of the actomyosin ring enables spermatocyte cytokinesis in *Drosophila*. *Mol. Biol. Cell*. 21:1482–1493. http://dx.doi.org/10.1091/mbc.E09-08-0714

Green, R.A., E. Paluch, and K. Oegema. 2012. Cytokinesis in animal cells. *Annu. Rev. Cell Dev. Biol.* 28:29–58. http://dx.doi.org/10.1146/annurev-cellbio-101011-155718

Gregory, S.L., S. Ebrahimi, J. Milverton, W.M. Jones, A. Bejsovec, and R. Saint. 2008. Cell division requires a direct link between microtubule-bound RacGAP and Anillin in the contractile ring. *Curr. Biol.* 18:25–29. http://dx.doi.org/10.1016/j.cub.2007.11.050

Gruneberg, U., R. Neef, X. Li, E.H. Chan, R.B. Chalamalasetty, E.A. Nigg, and F.A. Barr. 2006. KIF14 and citron kinase act together to promote efficient cytokinesis. *J. Cell Biol.* 172:363–372. http://dx.doi.org/10.1083/jcb.200511061

Haglund, K., I.P. Nezis, and H. Stenmark. 2011. Structure and functions of stable intercellular bridges formed by incomplete cytokinesis during development. *Commun. Integr. Biol.* 4:1–9.

Hickson, G.R., and P.H. O'Farrell. 2008a. Anillin: a pivotal organizer of the cytokinetic machinery. *Biochem. Soc. Trans.* 36:439–441. http://dx.doi.org/10.1042/BST0360439

Hickson, G.R., and P.H. O'Farrell. 2008b. Rho-dependent control of anillin behavior during cytokinesis. *J. Cell Biol.* 180:285–294. http://dx.doi.org/10.1083/jcb.200709005

Hu, C.K., M. Coughlin, and T.J. Mitchison. 2012. Midbody assembly and its regulation during cytokinesis. *Mol. Biol. Cell*. 23:1024–1034. http://dx.doi.org/10.1091/mbc.E11-08-0721

Kechad, A., S. Jananji, Y. Ruella, and G.R. Hickson. 2012. Anillin acts as a bifunctional linker coordinating midbody ring biogenesis during cytokinesis. *Curr. Biol.* 22:197–203. http://dx.doi.org/10.1016/j.cub.2011.11.062

Liu, J., G.D. Fairn, D.F. Ceccarelli, F. Sicheri, and A. Wilde. 2012. Cleavage furrow organization requires PIP(2)-mediated recruitment of anillin. *Curr. Biol.* 22:64–69. http://dx.doi.org/10.1016/j.cub.2011.11.040

Madaule, P., M. Eda, N. Watanabe, K. Fujisawa, T. Matsuoka, H. Bito, T. Ishizaki, and S. Narumiya. 1998. Role of citron kinase as a target of the small GTPase Rho in cytokinesis. *Nature*. 394:491–494. http://dx.doi.org/10.1038/28873

McKay, H.F., and D.R. Burgess. 2011. 'Life is a highway': membrane trafficking during cytokinesis. *Traffic*. 12:247–251. http://dx.doi.org/10.1111/j.1600-0854.2010.01139.x

Mullins, J.M., and J.J. Biesele. 1977. Terminal phase of cytokinesis in D-98s cells. *J. Cell Biol.* 73:672–684. http://dx.doi.org/10.1083/jcb.73.3.672

Naim, V., S. Imarisio, F. Di Cunto, M. Gatti, and S. Bonaccorsi. 2004. *Drosophila* citron kinase is required for the final steps of cytokinesis. *Mol. Biol. Cell*. 15:5053–5063. http://dx.doi.org/10.1091/mbc.E04-06-0536

Neto, H., L.L. Collins, and G.W. Gould. 2011. Vesicle trafficking and membrane remodelling in cytokinesis. *Biochem. J.* 437:13–24. http://dx.doi.org/10.1042/BJ20110153

Neufeld, T.P., and G.M. Rubin. 1994. The *Drosophila* peanut gene is required for cytokinesis and encodes a protein similar to yeast putative bud neck filament proteins. *Cell*. 77:371–379. http://dx.doi.org/10.1016/0092-8674(94)90152-X

Oegema, K., M.S. Savoian, T.J. Mitchison, and C.M. Field. 2000. Functional analysis of a human homologue of the *Drosophila* actin binding protein anillin suggests a role in cytokinesis. *J. Cell Biol.* 150:539–552. http://dx.doi.org/10.1083/jcb.150.3.539

Piekny, A.J., and M. Glotzer. 2008. Anillin is a scaffold protein that links RhoA, actin, and myosin during cytokinesis. *Curr. Biol.* 18:30–36. http://dx.doi.org/10.1016/j.cub.2007.11.068

Piekny, A.J., and A.S. Maddox. 2010. The myriad roles of Anillin during cytokinesis. *Semin. Cell Dev. Biol.* 21:881–891. http://dx.doi.org/10.1016/j.semcdb.2010.08.002

Pollard, T.D. 2010. Mechanics of cytokinesis in eukaryotes. *Curr. Opin. Cell Biol.* 22:50–56. http://dx.doi.org/10.1016/j.ceb.2009.11.010

Riedl, J., A.H. Crevenna, K. Kessenbrock, J.H. Yu, D. Neukirchen, M. Bista, F. Bradke, D. Jenne, T.A. Holak, Z. Werb, et al. 2008. Lifeact: a versatile marker to visualize F-actin. *Nat. Methods*. 5:605–607. http://dx.doi.org/10.1038/nmeth.1220

Schroeder, T.E. 1972. The contractile ring. II. Determining its brief existence, volumetric changes, and vital role in cleaving *Arbacia* eggs. *J. Cell Biol.* 53:419–434. http://dx.doi.org/10.1083/jcb.53.2.419

Sedzinski, J., M. Biro, A. Oswald, J.Y. Tinevez, G. Salbreux, and E. Paluch. 2011. Polar actomyosin contractility destabilizes the position of the cytokinetic furrow. *Nature*. 476:462–466. http://dx.doi.org/10.1038/nature10286

Shandala, T., S.L. Gregory, H.E. Dalton, M. Smallhorn, and R. Saint. 2004. Citron kinase is an essential effector of the Pbl-activated Rho signalling pathway in *Drosophila melanogaster*. *Development*. 131:5053–5063. http://dx.doi.org/10.1242/dev.01382

Smurnyy, Y., A.V. Toms, G.R. Hickson, M.J. Eck, and U.S. Eggert. 2010. Binucleine 2, an isoform-specific inhibitor of *Drosophila* Aurora B kinase, provides insights into the mechanism of cytokinesis. *ACS Chem. Biol.* 5:1015–1020. http://dx.doi.org/10.1021/cb1001685

Somma, M.P., B. Fasulo, G. Cenci, E. Cundari, and M. Gatti. 2002. Molecular dissection of cytokinesis by RNA interference in *Drosophila* cultured cells. *Mol. Biol. Cell*. 13:2448–2460. http://dx.doi.org/10.1091/mbc.01-12-0589

Steigemann, P., and D.W. Gerlich. 2009. Cytokinetic abscission: cellular dynamics at the midbody. *Trends Cell Biol.* 19:606–616. http://dx.doi.org/10.1016/j.tcb.2009.07.008

Straight, A.F., C.M. Field, and T.J. Mitchison. 2005. Anillin binds nonmuscle myosin II and regulates the contractile ring. *Mol. Biol. Cell*. 16:193–201. http://dx.doi.org/10.1091/mbc.E04-08-0758

Tanaka-Takiguchi, Y., M. Kinoshita, and K. Takiguchi. 2009. Septin-mediated uniform bracing of phospholipid membranes. *Curr. Biol.* 19:140–145. http://dx.doi.org/10.1016/j.cub.2008.12.030

Watanabe, S., T. De Zan, T. Ishizaki, and S. Narumiya. 2013. Citron kinase mediates transition from constriction to abscission through its coiled-coil domain. *J. Cell Sci.* 126:1773–1784. http://dx.doi.org/10.1242/jcs.116608

Yamashiro, S., G. Totsukawa, Y. Yamakita, Y. Sasaki, P. Madaule, T. Ishizaki, S. Narumiya, and F. Matsumura. 2003. Citron kinase, a Rho-dependent kinase, induces di-phosphorylation of regulatory light chain of myosin II. *Mol. Biol. Cell*. 14:1745–1756. http://dx.doi.org/10.1091/mbc.E02-07-0427

Zhao, W.M., and G. Fang. 2005. Anillin is a substrate of anaphase-promoting complex/cyclosome (APC/C) that controls spatial contractility of myosin during late cytokinesis. *J. Biol. Chem.* 280:33516–33524. http://dx.doi.org/10.1074/jbc.M504657200